

The Impact of aerosol–ice nuclei–cloud interactions on a Typical Spring Dust-Precipitation Event in China

Jian Zhang^{1,2}, Chunhong Zhou^{2*}, Xiaoyu Shen^{2,3}, Hong Wang^{2,4}, ~~Sunling Gong^{2,4}~~, Xiaoye Zhang^{2,4}

¹ Key Laboratory for Aerosol-Cloud-Precipitation of China Meteorological Administration, Nanjing

5 University of Information Science & Technology, Nanjing, Jiangsu, China

² Institute of Atmospheric Composition and Environmental Meteorology & Key Laboratory of Atmospheric Chemistry of CMA, Chinese Academy of Meteorological Sciences, Beijing, China

³ Key Laboratory of Urban Air Particulate Pollution Prevention and Control of Ministry of Ecology and Environment, College of Environmental Science and Engineering, Nankai University, Tianjin, China

10 ⁴ State Key Laboratory of Severe Weather, Chinese Academy of Meteorological Sciences, Beijing, China

* Corresponding authors.

E-mail addresses: zhouch@cma.gov.cn (Chunhong Zhou)

15 Abstract.

To investigate the impact of ice nuclei (IN) activated by dust aerosols on precipitation over China, this study uses regional Global/Regional Assimilation and Prediction System – China Meteorological Administration Unified Atmospheric Chemistry Environment (GRAPES/CUACE). The original temperature-dependent IN nucleation scheme in the Double-Moment 6-Class (WDM6) is improved by incorporating an on-line aerosol–IN nucleation scheme to examine their effects during a typical dust affected precipitation event in East Asia.~~The original temperature-dependent IN nucleation scheme is improved by incorporating an on line aerosol IN nucleation scheme. The INs are fed on line into the Double Moment 6 Class (WDM6) cloud microphysics scheme in a typical dust affected precipitation event in East Asia.~~

25 Dust~~The on line aerosol IN nucleation scheme~~ modifies the spatial distribution and number concentration~~density~~ of IN, affecting heterogeneous ice nucleation. Compared with the systematic underestimation in original WDM6, the peak values of nucleated INs can reach $10^{-4} L^{-1}$ ~~INs reach $10^3 - 10^4 L^{-1}$~~ with the improved scheme, which is closer to observations. ~~and cloud ice is reasonably formed between 2 and 6 km in height.~~

30 Dust inhibit the development of clouds. Above 7 km, dust suppresses both

Formatted: Default Paragraph Font, Font: (Default) Times New Roman, (Asian) +Body Asian (等线), Not Bold, Font color: Black, (Asian) Chinese (Simplified, Mainland China)

Formatted: Font: (Asian) +Body Asian (等线), (Asian) Chinese (Simplified, Mainland China)

35 heterogeneous nucleation and deposition growth. Thus, the total production rate of
cloud ice drops to less than 24% of that in the control test T_CTL, promoting snow
formation and reducing the total ice-phase hydrometeor content to 70–85% of T_CTL.
Between 4 and 7 km, dust enhances heterogeneous nucleation of cloud ice but
suppresses deposition growth, leading to a decrease in the total ice-phase hydrometeor
content to 85–91% of T_CTL. Below 4 km, dust suppresses the conversion of water
40 vapor to cloud water, thereby reducing the liquid-phase hydrometeor content to 90–95%
of T_CTL. The scheme alters the distribution of cloud hydrometeors, making it closer
to observations. Above the freezing level, the ice-phase hydrometeors mixing ratio
decreases due to the higher cloud-top temperatures in dusty weather. And the ratio of
cloud-ice to cloud-snow changes from 1:1 to 1:3. Near the freezing level, increased
cloud-ice converts to cloud-water, resulting in its increasing. During the dust-
45 precipitation event, rainwater is decreased due to vapor-competition between IN and
cloud-condensation nuclei.

Dust modifies the precipitation distribution, bringing it closer to observations. The
scheme also modulates the precipitation distribution closer to observations. It
suppresses precipitation near dust source areas, where mean-accumulated precipitation
50 decreased by about 44.5 mm, while the downstream event-mean precipitation increased
by about 1.10-18 mm.–

Formatted: Not Highlight

Formatted: Not Highlight

Keywords: aerosol–IN–cloud–precipitation interactions; dust–precipitation event;
on-line aerosol–IN nucleation scheme, CUACE

55 **1 Introduction**

The formation of cloud ice is one of the key processes in ice-phase precipitation, and ice nuclei (IN) ~~associated with~~~~involving~~ aerosols play a crucial role in the development of cloud ice, particularly in mid- to high-latitude areas and in the upper troposphere (Li et al., 2022; Chen et al., 2023; Knopf and Alpert, 2023). This is because
60 homogeneous nucleation without IN occurs only below $-40\text{ }^{\circ}\text{C}$, which ~~is~~~~are~~ relatively rare in natural atmospheric environments (Eastwood et al., 2008a; Herbert et al., 2015; Kumar et al., 2020; Che et al., 2021). In contrast, ~~heterogeneous nucleation mediated by IN~~~~heterogeneous nucleation involving IN~~ can occur under ice-supersaturated conditions at much higher temperatures, ~~making it the dominant pathway for cloud ice formation.~~
65 ~~Therefore, heterogeneous nucleation mediated by IN is the dominant pathway for cloud ice formation.~~

Aerosols can ~~serve as~~~~act as~~ IN, participating in cloud formation, altering cloud microphysical properties and lifetimes, ~~and~~ thereby affecting precipitation (Albrecht, 1989; Andreae and Crutzen, 1997). Among different species, mineral dust is recognized
70 as one of the primary sources of atmospheric IN (Khain et al., 2000; Nenes et al., 2014; Tobo et al., 2019). Dust particles have unique surface structures that facilitate the adsorption and binding of water molecules, promoting the formation of cloud ice (Possner et al., 2017; Stevens et al., 2018). Stith et al. (2009) and DeMott et al. (2015) have found a ~~strong~~~~high~~ correlation between IN number concentration and aerosols
75 with diameters larger than $0.5\text{ }\mu\text{m}$, with mineral dust accounting for 33-50% of the total IN. Jiang et al. (2016) ~~observed~~~~found~~ that IN concentrations observed during dust events in Huangshan, ~~Xinjiang~~ and Nanjing were significantly higher than those ~~during~~
~~under~~ non-dust conditions. Tobo et al. (2020) observed that IN concentrations increased remarkably during dust events in Tokyo when temperatures were above $-25\text{ }^{\circ}\text{C}$. In
80 addition, aged dust aerosol has increased solubility, which can act as cloud condensation nuclei (CCN) and thereby further influencing precipitation (Trochkin et al., 2003).

Compared with the relatively well-understood impacts of aerosols as CCN, the role of dust as IN is considerably more complex and remains poorly understood, with

Formatted: Font color: Black

Formatted: Font: (Asian) 宋体, Font color: Black

Formatted: Font: (Asian) 宋体, Font color: Black

Formatted: Font: (Asian) 宋体, Font color: Black

Field Code Changed

Field Code Changed

Formatted: Not Highlight

Formatted: Not Highlight

Formatted: Font color: Auto, Not Highlight

85 ~~substantial uncertainties (Kaufman et al., 2002; Eastwood et al., 2008b; Pan et al., 2017; Possner et al., 2017). Observational studies have reported diverse and sometimes contradictory relationships between dust and precipitation, depending on temporal scale, season, and environmental conditions. Temporal scale and seasonality play a critical role in shaping the observed relationships between dust and precipitation. At~~
90 ~~interannual scales. Han et al. (2008) found a significant negative correlation between dust storm frequency and precipitation over the Taklimakan Desert, whereas a positive correlation was observed at monthly scales, suggesting that dust-precipitation relationships are scale dependent. Seasonal contrasts have also been reported. Using long-term ground-based observations, Wang (2013) showed that dust aerosols tend to~~
95 ~~suppress precipitation over arid and semi-arid regions in spring but may enhance precipitation in summer. In addition to temporal variability, the impacts of dust on clouds and precipitation also exhibit strong regional and environmental dependence. In contrast, Naeger (2018) found that dust could enhance precipitation over Florida based on multi-sensor satellite observations and field campaigns. More recently, Hu et al. (2023) demonstrated that the impact of springtime dust on precipitation is strongly modulated by the presence of other aerosol types. Liu et al. (2024) analyzed the spatiotemporal patterns and trends of dust aerosols and precipitation and found that dust~~
100 ~~increases suppress precipitation over source regions such as the Gobi and Taklamakan deserts, but enhance precipitation in downwind areas like northern China. Overall, due to the multiple factors influencing precipitation beyond aerosols, it remains challenging to quantify the impact of dust on precipitation from observations alone (Zhou et al., 2016; Stier et al., 2024), highlighting the need for process-oriented numerical modeling studies with physically based aerosol-ice nucleation parameterizations. Compared with the relatively well-understood impacts of aerosols as CCN, the role of dust as IN is~~
105 ~~considerably more complex and remains poorly understood, with substantial uncertainties (Kaufman et al., 2002; Pan et al., 2017). From statistical studies, Han et al. (2008) found that precipitation events often co occur with dust storm in the Taklimakan Desert, showing a significant negative correlation between dust storm~~
110

Formatted: Font color: Auto, Not Highlight

Formatted: Font color: Auto, Not Highlight

Formatted: Font color: Auto, Not Highlight

Formatted: Font color: Auto, Not Highlight

Formatted: Font color: Auto, Not Highlight

Formatted: Font color: Auto, Not Highlight

Formatted: Font color: Auto, Not Highlight

Formatted: Font color: Auto, Not Highlight

Formatted: Font color: Auto, Not Highlight

Formatted: Font color: Auto, Not Highlight

Formatted: Font color: Auto, Not Highlight

Formatted: Font color: Auto, Not Highlight

Formatted: Font color: Auto, Not Highlight

115 frequency and precipitation at interannual scales but a positive correlation at monthly
120 scales. Based on observations data from Semi Arid Climate and Environment
125 Observatory of Lanzhou University, Wang (2013) found that dust aerosols tend to
suppress precipitation over arid and semi-arid areas in spring, while promoting it in
summer. From Observational studies, satellite and aircraft measurements by Rosenfeld
and Bell (2011) found that dust had little impact on total cloud water content but reduces
cloud droplet effective radius and precipitation efficiency. Naeger (2018) found that dust
could enhance precipitation over Florida through multi-sensor satellite observations and
field campaigns. Hu et al. (2023) found that the influence of springtime dust on
precipitation was modulated by other aerosols. Overall, due to the multi factors
influencing precipitation beyond aerosols, it remains challenging to quantify the impact
of dust on precipitation by observational solely (Zhou et al., 2016; Stier et al., 2024).

Numerical model is a crucial approach for numerically studying the impact of dust
on precipitation. In early cloud microphysics scheme, the ice nucleation scheme did not
account for aerosols, with IN concentrations typically expressed as functions of
temperature or supersaturation (DeMott et al., 2010). Moreover, many clouds ice
130 microphysical schemes were single-moment, which only simulated the mass mixing
ratio of cloud ice. ~~Such~~ This single-moment schemes often led to large biases in cloud
ice mass concentrations (Molthan and Colle, 2012; Igel et al., 2015). In contrast,
double-moment ice schemes, ~~which -that~~ simulate both cloud ice mass and number
concentrations-, ~~outperform the single-moment schemes in terms of the simulated~~
135 ~~structure, life cycle, cloud coverage, precipitation, and microphysical properties~~
~~provide more accurate cloud ice particle size distributions and concentrations that are~~
~~more consistent with MODIS satellite observations~~ (Pu and Lin, 2015; Zhao et al., 2021).
The double-moment ice schemes can provide more stable and improved precipitation
simulations (Kang et al., 2018; Shen et al., 2022; Shen et al., 2024). Mascioli et al.
140 (2021) used the Thompson aerosol-aware microphysics scheme, incorporating the IN
nucleation scheme of DeMott et al. (2010), to study the sensitivity of precipitation to
different prescribed dust aerosol concentrations. Park and Lim (2023) ~~develops the~~

Formatted: Font color: Auto
Formatted: Font color: Auto

Formatted: Font color: Auto
Formatted: Font color: Auto

Formatted: Font color: Auto
Formatted: Font color: Auto

Formatted: Font color: Auto
Formatted: Font color: Auto
Formatted: Font color: Auto
Formatted: Font color: Auto
Formatted: Font color: Auto
Formatted: Font color: Auto
Formatted: Font color: Auto

145 ~~revised Weather Research and Forecasting Double-Moment 6-class (WDM6) scheme through the implementation of prognostic cloud ice number concentrations implemented a cloud ice microphysics scheme in the Weather Research and Forecasting Double Moment 6-class (WDM6) microphysics scheme and examined the influence of dust on precipitation using aerosol diffusion coefficients. The excess generation of cloud ice mixing ratio is considerably alleviated. Their results suggested that dust could modulate the spatial distribution of precipitation.~~ However, these studies

150 did not establish an explicit quantitative relationship between on-line aerosols and IN. ~~Su and Fung (2018a)~~ implemented the simplified Goddard Chemistry Aerosol Radiation and Transport aerosol model (GOCART) together with Shao's dust emission scheme ~~(Kang et al., 2011; Shao et al., 2011)~~ in WRF/Chem and incorporated the online IN nucleation scheme of ~~DeMott et al. (2015)~~ for producing real time ~~of~~ IN into the

155 double-moment Thompson–Eidhammer microphysics scheme. They analyzed the impact of dust ~~in East Asia~~ on radiative forcing ~~together with~~ and temperature ~~in East Asia very carefully, and but thus~~ only the sensitive impacts in terms of precipitation rate in March and April in 2012 ~~(Su and Fung, 2018b)~~. The spring of 2012 is not a typical dust season, most dust storm concentrated in Mongolia. ~~Therefore, the microphysical pathways through which dust affects precipitation during typical dust events remain insufficiently studied. In this study, we focus on a representative spring dust-precipitation event and explicitly examine the cloud microphysical processes associated with dust-induced heterogeneous ice nucleation, together with direct comparisons to precipitation observations i~~ ~~And their work needs more comparison with real precipitation observations.~~

160 ~~In this study, we also employ~~ the Global/Regional Assimilation and PrEdiction System, China Meteorological Administration (CMA) Unified Atmospheric Chemistry Environment (GRAPES/CUACE) model ~~to investigate the effects of dust aerosols on precipitation.~~ GRAPES/CUACE provides on-line sectional aerosol concentrations with

170 multi chemical composition information ~~(Wang et al., 2010; Zhou et al., 2012)~~. Zhou et al. (2016) ~~introduced an on-line aerosol–CCN–cloud interaction scheme into the system,~~

Formatted: Font color: Auto

Formatted: Font color: Auto

Formatted: Font color: Auto

Formatted: Font color: Auto

Formatted: Font color: Auto

Formatted: Font color: Auto

Formatted: Font color: Auto

Formatted: Font color: Auto

Formatted: Font color: Auto, Not Highlight

Formatted: Font color: Auto

Formatted: Font color: Auto

Formatted: Font: (Asian) 宋体

Formatted: Font color: Auto

Formatted: Font color: Auto

Formatted: Font color: Auto

Formatted: Font color: Auto

allowing the model to simulate real time CCN activation and their influence on precipitation. However, in the GRAPES/CUACE microphysics scheme WDM6, IN is a function of temperature only, and cloud ice is represented by a single-moment scheme only for the mass mixing ratio (Hong et al., 2004; Hong et al., 2006; Zhang et al., 2022).

To address these limitations, this study implements a double-moment cloud ice scheme and incorporates an on-line aerosol-IN nucleation scheme to explicitly represent heterogeneous processes. Using this improved framework, we then investigate the impact of dust on precipitation by a typical dust affected precipitation event in East Asia.

This paper is organized as follows: Section 2 introduces the model configuration, cloud microphysical processes, on-line aerosol-IN nucleation scheme, study region, and observational datasets. Section 3 presents the evaluation of the improved model's simulation performance and discusses the effects of dust on precipitation. Section 4 summarizes the main conclusions of the study.

2 Model description and methodology

2.1 GRAPES/CUACE

The GRAPES is a fully compressible, non-hydrostatic numerical weather model that adopts a semi-implicit and semi-Lagrangian discretization scheme (Chen et al., 2008; Xu et al., 2008; Zhang and Shen, 2008; Wang et al., 2022a). The physical packages include cumulus convective, single-moment cloud microphysics, radiative, land surface, and boundary layer processes. CUACE is a regional chemical weather forecasting system developed by Gong and Zhang (2008) coupled on-line with GRAPES (Wang et al., 2010). It is capable of simulating on-line seven aerosol species of sulfate, nitrate, ammoniumammonia, black carbon, organic carbon, sea-salt together with dust (Zhou et al., 2008, 2012; Wang et al., 2015). The sectional dust emission scheme is by Marticorena and Bergametti (1995) and Alfaro and Gomes (2001) which has been improved by surface dust flux observations and desertification in East Asia (Gong et al., 2003), and new desertification map and soil texture samples from Chinese deserts (Zhou et al., 2019; Zhou et al., 2024). The aerosol size spectra have been divided into 12 size bins with a radius range of 0.005–0.01, 0.01–0.02, 0.02–0.04, 0.04–0.08,

Formatted: Font color: Auto

Formatted: Font color: Auto

Formatted: Font color: Auto

Formatted: Font color: Auto

Formatted: Font: (Asian) 宋体, (Asian) Chinese (Simplified, Mainland China)

Formatted: Font: (Asian) 宋体

0.08–0.16, 0.16–0.32, 0.32–0.64, 0.64–1.28, 1.28–2.56, 2.56–5.12, 5.12–10.24, and 10.24–20.48 μm . ~~GRAPES/CUACE~~The model has a horizontal resolution of 0.15° and 31 vertical levels extending to approximately 28.6 km in altitude.

2.2 WDM6 microphysics scheme

In this study, we select the WDM6 microphysics scheme in GRAPES for simulating precipitation (Hong et al., 2004; Zhang et al., 2022). The WDM6 scheme simulates the mass mixing ratio of water vapor (Q_v), as well as the mass and number concentrations of cloud water (Q_c) and ~~rainwater~~cloud-rain (Q_r) in warm clouds. For icy clouds, it includes the mass mixing ratios of cloud ice (Q_i), snow (Q_s), and graupel (Q_g). A double-moment cloud ice scheme by Park and Lim (2023) is incorporated into the WDM6 scheme, allowing for the explicit prediction of cloud ice number concentration in GRAPES. A sectional CCN activated scheme has been introduced in ~~WDM6 in GRAPES/CUACE~~GRAPES, connecting the multi-component multi-section aerosols from CUACE into the WDM6 microphysics and the sub-grid convective parameterization scheme by newly activated CCN at each time step (Zhou et al., 2016). ~~Thus a fully aerosol-CCN-cloud interaction scheme has been implemented in GRAPES/CUACE.~~

2.3 On-line aerosol-IN nucleation scheme

In the original WDM6 scheme, when the temperature is below 0°C , the production rate of cloud ice is attributed to two processes: ~~heterogeneous nucleation (P_{igen}) and deposition-sublimation rate of cloud ice (P_{idep}). Both consume water vapor to form ice clouds.~~nucleation of ice from vapor (P_{igen}) and deposition sublimation (P_{idep}). The abbreviations for the remaining cloud microphysical processes are listed in Table 2. The IN concentration is calculated by a classical ice nuclei nucleation scheme, which is an empirical function of temperature and does not account for the influence of atmospheric aerosols (Hong et al., 2004):

$$N_{ice}(m^{-3})=10^3 e^{0.1(T_0-T_k)} \quad (1)$$

Where, T_k is atmospheric temperature, T_0 is the freezing point (273.15 K).

Formatted: Font: (Asian) 宋体, Font color: Black, (Asian) Chinese (Simplified, Mainland China), Pattern: Clear

Formatted: Font: (Asian) 宋体, Font color: Auto, Pattern: Clear

Formatted: Font color: Auto

Formatted: Font: Not Bold

Formatted: Font: 10 pt, (Asian) Chinese (Simplified, Mainland China)

Formatted: Not Highlight

This ~~study~~ ~~study implements~~ ~~aims to implement~~ an on-line aerosol-IN nucleation scheme in GRAPES/CUACE that accounts for heterogeneous ice nucleation processes influenced by atmospheric aerosols. Heterogeneous nucleation mechanisms are generally classified into immersion freezing, condensation freezing, deposition nucleation, and contact freezing (Hiranuma et al., 2015; Ilotoviz et al., 2016; Lee et al., 2017). Among these mechanisms, immersion freezing, condensation freezing, and deposition nucleation are selected, as they are relatively well developed. This selection is based on the fact that dust aerosols primarily affect ice nucleation at temperatures below 258.15 K through these three mechanisms (Cantrell et al., 2013; Patnaude et al., 2025), whereas the efficiency of contact freezing by dust particles is relatively low (Niehaus et al., 2014). ~~the first three of them are selected which are relatively well developed. And the reasons to choose the three are also that dust aerosols affect ice nucleation mainly at temperatures below 258.15 K through the three (Cantrell et al., 2013; Patnaude et al., 2025), and the efficiency of contact freezing by dust particles is relatively low (Niehaus et al., 2014).~~

Immersion freezing is a heterogeneous ice nucleation process with existence of liquid drops at temperatures between 233.15 K and 273.15 K, which ice nucleus immersed in supercooled liquid, triggering it freezing into an ice crystal (Boose et al., 2016). Immersion freezing consumes water vapor to form cloud ice. The initial size of the ice crystal is influenced by the size of the liquid droplet (Fan et al., 2014; Gibbons et al., 2018), therefore the cloud ice formation through this mechanism is relatively easier compared to other nucleation ~~mechanisms~~ ~~modes~~. The selected ~~In this study, the~~ immersion freezing nucleation scheme used here is developed by DeMott et al. (2015), based on continuous flow diffusion chamber measurements. The number concentration of ice nuclei, N_{icenui} , activated via immersion freezing is given by:

$$N_{icenui}(\text{m}^{-3}) = 3 * n_{aer,0.5}^{1.25} * e^{(0.46*(273.16-T_k)-11.6)} \quad (2)$$

Where, $n_{aer,0.5}^{1.25}$ is the number concentration of insoluble aerosol particles with diameters exceeding 0.5 μm such as dust, black carbon and part of organic carbon. ~~At~~ is the integration time step.

Field Code Changed

Deposition and condensation freezing are both heterogeneous ice nucleation processes that occur at temperatures between 248.15 K and 258.15 K (Chen et al., 2019).

Field Code Changed

In condensation freezing, water vapor first condenses on the surface of IN and subsequently freezes to form an ice crystal, while in deposition nucleation, water vapor directly deposits onto the IN surface (Kanji et al., 2017). The initial size of the ice crystals is comparable to that of the smallest droplets (Chen et al., 2019), and the ice formation through these two pathways is generally harder than that through immersion freezing (DeMott et al., 2015). In this study, the parameterization scheme selected here is developed by Jiang et al. (2016) and (Chen et al., 2019) is adopted. It first developed by Jiang et al. (2016), based on which was derived from dust events observed in Xinjiang, Huangshan, and Nanjing in China, using the static vacuum vapor diffusion chamber Frankfurt Ice nucleation Deposition freezing Experiment. Then some parameters of it was refined and extended it to represent both deposition and immersion freezing by Chen et al. (2019). The number concentration of ice nuclei, N_{icenu} by combines both deposition and condensation freezing is as processes into the following:

Formatted

$$N_{icenu} = 5.7 * 10^{-7} n_{aer,0.5}^{0.018(273.16-Tk)-0.007S_i+0.342} * (273.16 - Tk)^{3.745} * S_i^{1.31} \quad (3)$$

Where, S_i is supersaturation with respect to ice.

WDM6 uses the formula $\rho q_{i0}(kg m^{-3}) = 4.92 \times 10^{-11} N_{ice}^{1.33}$ and $P_{igen}(kg kg^{-1} s^{-1}) = \frac{(q_{i0}-q_i)}{\Delta t}$ to calculate newly nucleation of ice. Where, ρ denotes the newly-formed air density, and q_{i0} is the predicted ice mixing ratio ($kg kg^{-1}$). Δt is the integration time step. Production rate for heterogeneous nucleation is calculated as the difference between q_{i0} and the current ice mixing ratio (q_i). However, it does not account for the influence of nucleated IN size or the specific characteristics of different heterogeneous ice nucleation mechanisms on ice crystal development.

Formatted: Not Highlight

Formatted

Formatted

Formatted

Formatted

Formatted

Formatted

Formatted

WDM6 uses the formula $\rho q_{i0}(kg m^{-3}) = 4.92 \times 10^{-11} N_{ice}^{1.33}$ to calculate nucleation of ice from vapor due to the IN increase. It ignores the influence of IN size and heterogeneous ice nucleation processes. Here, the mass production rate of cloud ice newly nucleated is calculated as the following:

Formatted: Not Highlight

Then, the original production rate for nucleation of ice from vapor P_{igen} in WDM6 is replaced by the ~~deposition/condensation-freezing~~ P_{inud} and ~~immersion freezing~~ P_{inui} described above.

2.4 Case description and test design

The typical dust affected precipitation event

The typical dust affected precipitation event is from 00:00 UTC on 9 April to 00:00 UTC on 15 April 2018, which contains two dust storms events in East Asia. One is from 9 to 11 April, originating in Mongolia and affected northern China. Lots of dust storm phenomena are observed in Mongolia, while blowing dust and floating dust phenomena are reported in central and western Inner Mongolia, central Gansu, Ningxia, northern Shaanxi, most parts of Shanxi, southern Hebei, northern Henan, and western Shandong in China (see Fig. S1 for locations). Another event is from 13 to 14 April. It also gains with widespread dust storm phenomena in Mongolia and central Inner Mongolia, blowing or floating dust phenomena observed in central Inner Mongolia, northern Shanxi, Beijing, Tianjin, and northern Hebei in China. Between the two dust storm events, the precipitation occurred from west to east covering most of northern China extending to the Yangtze River area, from 00:00 UTC on 12 April to 00:00 UTC on 15 April, with the highest accumulations concentrated in Shaanxi, Henan, southern Hebei, and along the Yangtze River in Sichuan, Hubei, Anhui, and the Jiangsu-Zhejiang-Shanghai area.

Figure 1a presents the dust-affected areas by dust phenomenon from Meteorological stations and PM_{10} from the National Environmental Monitoring Network of the Ministry of Environmental Protection. Based on the distribution of dust in this event, the domain bounded by 90-135 °E and 20-54 °N is defined as the major dust-affected area (DA, outer red rectangle in Figure 1). Together with the real precipitation distribution (Fig. 5a), the domain ~~bounds-bounded~~ by 103°-130.5°E and 27.5°-50°N is defined as the dust-affected precipitation (DP) area (DPA, the inner red rectangle in Figure 1). The whole model domain covers 70°-145°E and 15°-64.5°N, containing the DA and DPA. To investigate the impact of dust on precipitation in

Formatted: Font: 10 pt, (Asian) Chinese (Simplified, Mainland China)

Formatted: Font: 10 pt, Font color: Black, (Asian) Chinese (Simplified, Mainland China)

Formatted: MDPL_2.1_heading1, Line spacing: single

regions distant from the dust source in Section 3.3, we calculate horizontal hydrometeor fluxes across 116°E (33°–50°N) and 33°N (103°–116°E) during 12:00 UTC on 12 April to 18:00 UTC on 13 April (Fig. 6).

340 –GRAPES/CUACE successfully reproduces both the spatial distribution and intensity of the dust events (Fig. 1b). Considering that many radar observations and model studies have indicated that dust mainly participates in within the mid-tropospheric layer (-20 - 0 °C) cloud-ice processes between 3-4 and 7-5 km in altitude (Haarig et al., 2019; He et al., 2021; He et al., 2023), Fig. 1c also shows the simulated dust within this the 3-5 km altitude range layer.

Test design

350 As shown in Table 1, three tests are designed. The first test uses the original WDM6 microphysics scheme without considering aerosol effects, denoted as T_CTL. The second test incorporates the on-line aerosol-CCN-cloud interaction scheme from Zhou et al. (2016), denoted as T_CCN. Based on T_CCN, the third test adds the on-line aerosol-IN nucleation scheme described in Section 2.3, denoted as T_CCNIN. As shown in Table 1, two tests are designed. The first test uses the on-line aerosol-CCN-cloud interaction scheme from Zhou et al. (2016), denoted as T_CTL. Based on T_CTL, the second test adds the on-line aerosol-IN nucleation scheme described in Section 2.3, denoted as T_IN.

The successive integration is cut into several three-days-interval with a warm restart. It starts at 00:00 UTC on April 5, 2018 with 6 days spinning up for tracers in CUACE. As simulation time increases, integration errors tend to accumulate (Zhang et al., 2019), and to minimize the influence of initial conditions on precipitation, the simulations in this study were divided into several time segments: 5–8 April, 8–11 April, 11–14 April, and 13–16 April. Among these, the simulation results for 13 April were taken from the 11–14 April experiment to minimize the influence of initial conditions on precipitation development. Except for water vapor, all initial values of hydrometeors are zero for each run. The model outputs 1-hourly precipitation data. To compare with the observed 6-hourly precipitation, the model outputs are temporally interpolated to

Field Code Changed

Formatted: Not Highlight

Formatted: Not Highlight

Formatted: Not Highlight

Formatted: Not Highlight

~~the time stamps of the observations. The outputs are in 3-hour interval. As simulation time increases, integration errors tend to accumulate (Zhang et al., 2019), and to minimize the influence of initial conditions on precipitation, an additional test is conducted from 11 to 13 April. Then the results on April 13 are taken from this test.~~

370 The initial and boundary meteorological conditions for GRAPES/CUACE are from the Final Operational Global Analysis data produced jointly by the National Centers for Environmental Prediction (NCEP) and the National Center for Atmospheric Research (NCAR) ~~in-at~~ a temporal resolution of 6 hours and a spatial resolution of 0.15°. The anthropogenic emissions are from Multi-resolution Emission Inventory for China (Li
375 et al., 2017).

2.5 Data and evaluation methodology

~~The initial and boundary meteorological conditions for GRAPES/CUACE are obtained from the NCEP/NCAR Final Operational Global Analysis (FNL) data, with a temporal resolution of 6 hours and a spatial resolution of 0.25°. Dust observations are~~
380 obtained from two sources: weather phenomena from the CMA surface meteorological observation network with a temporal resolution of 3 hours, while PM₁₀ and PM_{2.5} concentration data from the national environmental monitoring network of the Ministry of Ecology and Environment of China, with a temporal resolution of 1 hour. 6-hour ~~accumulated~~ rainfall data are also from CMA surface meteorological observation
385 network. As there are more than 2,000 precipitation stations in DA, only 63 stations ~~with quality-of~~ levels 1 and 2 ~~evenly distributed~~ are selected for evaluation, ~~in-of~~ which 43 stations are in DPA to avoid overfitting with the model outputs. Due to the complex sources of PM₁₀ and considering the ~~relatively~~relative long atmospheric residence time
of dust, we select precipitation stations where the PM_{2.5}/PM₁₀ ratio is less than 0.6
390 within 24 hours prior to the precipitation event as representative of dust-influenced precipitation (DP) stations (Wang and Yan, 2007; Filonchik et al., 2019).

Model performance is evaluated using mean absolute error (MAE), root mean square error (RMSE), and symmetric mean absolute percentage error (sMAPE) (Shcherbakov et al., 2013):

Formatted: Font: (Asian) 宋体, 小四, Font color: Auto, Not Highlight

$$\begin{aligned}
MAE &= \frac{\sum_{i=1}^n (r_{mi} - r_{oi})^2}{n} & (8) \\
RMSE &= \sqrt{\frac{\sum_{i=1}^n (r_{mi} - r_{oi})^2}{n}} \\
sMAPE &= \frac{1}{n} \sum_{i=1}^n \frac{|r_{mi} - r_{oi}|}{|r_{mi}| + |r_{oi}|} \\
aMAPE &= \frac{r_{mi} - r_{oi}}{|r_{mi}| + |r_{oi}|}
\end{aligned}$$

395 where r_{mi} represents the simulated cumulative precipitation at station i , and r_{oi} denotes the observed precipitation. For MAE, RMSE and sMAPE, values closer to 0 indicate better simulation performance. The aMAPE is used to evaluate whether the simulated precipitation is overestimated or underestimated compared with the observation. When $aMAPE > 0$, the precipitation is overestimated; when $aMAPE < 0$, the precipitation is underestimated. $aMAPE = \frac{r_{mi} - r_{oi}}{|r_{mi}| + |r_{oi}|}$ is used to evaluate overestimation and underestimation of the impact. When $aMAPE < 0$, precipitation is underestimated, and vice versa.

Formatted: Not Highlight

Formatted: Not Highlight

3 Results

3.1 Ice nuclei

405 During the DP event, the implemented on-line aerosol-IN nucleation scheme enables dust aerosols to modify the nucleated IN number concentration. Figures 2a and 2b show the horizontal distribution of the maximum nucleated IN number concentration between 4 and 7 km above ground level at DP stations during the time period from 00:00 UTC on 11 April to 00:00 UTC on 15 April 2018 for T_CTL and T_IN, respectively. Figure 2c presents the vertical distribution of DP-event-averaged production rate for Nigen for T_CTL (red line) and T_IN (blue line). Figure 2d presents the vertical distribution of cloud ice mass production rate for heterogeneous ice nucleation for T_CTL and T_IN. Based on the variation characteristics, the vertical layer is divided into three parts: layer A, above 7 km (temperature below -18°C); layer B, between 4 and 7 km (temperature approximately -18°C to -1.5°C); and layer C, below 4 km (temperature approximately -1.5°C to 18°C).

Formatted: Not Highlight

Formatted: Not Highlight

Formatted: Not Highlight

The on-line aerosol-IN nucleation scheme can correct the systematic

underestimation of IN concentrations. The maximum nucleated IN number concentrations in T_CTL can reach 10^2 L^{-1} in layer B during the DP event (Fig. 2a), showing a relatively uniform horizontal pattern, which is much lower than observed IN concentrations ($10^2\text{--}10^4 \text{ L}^{-1}$) during East Asian dust events (Bi et al., 2019; Tobo et al., 2019; Chen et al., 2021; Hu et al., 2023). The DP-event-averaged production rate for nucleated IN number concentration ranges $0.005\text{--}0.01 \text{ L}^{-1} \text{ S}^{-1}$ in layer B (Fig. 2c). In T_CTL, the production rate for nucleated IN number concentration increases with height (Fig. 2c), primarily due to the temperature-dependent nature of original WDM6 scheme. As a result, cloud ice mass production rate due to heterogeneous ice nucleation peak near the -40°C level (Fig. 2d). Above this layer, IN concentration continues to increase, but production rate of heterogeneously nucleated cloud ice begins to decline due to limited water vapor (Fig. 2d).

In T_IN, the maximum nucleated IN number concentrations can reach 10^4 L^{-1} in layer B during the DP event (Fig. 2b), closer to those observed or simulated in other East Asian dust events (Bi et al., 2019; Tobo et al., 2019; Chen et al., 2021; Hu et al., 2023). The DP-event-averaged production rate for nucleated IN number concentration ranges from 0.2 to $3.7 \text{ L}^{-1} \text{ S}^{-1}$ in layer B (Fig. 2c), and the cloud ice mass production rate for heterogeneous ice nucleation also peaks in this layer, which is consistent with radar observations and other modeling studies (Haarig et al., 2019; He et al., 2021; He et al., 2023). As immersion freezing is the dominant heterogeneous nucleation mechanism (DeMott et al., 2015; Hiranuma et al., 2015), the production rate of IN produced by it can exceed that of deposition and condensation freezing by 4–5 orders and the production rate of cloud ice by 5–6 orders in DP-event-averaged.

Figures 2a and 2b show the horizontal distribution of the maximum IN number concentration between 3 and 5 km above ground level in DPA area during 00:00 UTC on 11 April to 00:00 UTC on 15 April 2018 by T_CTL and T_CCNIN, respectively. Figure 2c presents the vertical distribution of number concentrations of dust with diameters larger than $0.5 \mu\text{m}$ and IN number concentrations averaged over all DPA stations. Figure 2d shows the vertical distribution of production rate for nucleation of

Formatted: Superscript

Formatted: Font: (Default) Times New Roman

Field Code Changed

Formatted: Font: (Default) Times New Roman

Field Code Changed

Formatted: Font: (Default) Times New Roman

Formatted: Not Highlight

Formatted: Not Highlight

Formatted: Not Highlight

Formatted: Not Highlight

Formatted: Not Highlight

ice. Both the IN number concentration and the production rate for nucleation of ice are calculated at one model time step (100 s).

The on-line aerosol-IN nucleation scheme can correct the systematic underestimation of IN concentrations. The IN distribution in T_{CCN} is similar to that in T_{CTL}, with IN concentrations ranging around 10^3 – 10^4 L⁻¹ between the altitude of 3 and 5 km during the DP event (Fig. 3a), showing a relatively uniform horizontal pattern. The IN concentration increases with height (Fig. 3c), primarily due to the temperature-dependent nature of original WDM6 scheme. As a result, cloud ice is mainly produced near the -40 °C level. Above this layer, IN concentration continues to increase, but production rate for nucleation of ice begin to decline due to limited cloud water (Fig. 3d). In T_{CCNIN}, the DP event averaged IN concentrations can reach 10^3 – 10^4 L⁻¹ and higher near the source area, about 90% from dust aerosol, closer to those observed or simulated in other East Asian dust events (Tobo et al., 2020; Hu et al., 2023; Herbert et al., 2025). The vertical distribution of IN is clearly influenced by both the dust concentration and water/ice saturation (Fig. 3b). At altitudes up to 6 km, both the IN concentration and cloud water decrease (Fig. 3c), and the production rate for nucleation of ice peaks between 4 and 5 km (Fig. 3d) which is consistent with radar observations and other modeling studies (Haarig et al., 2019; He et al., 2021; He et al., 2023).

3.2 Hydrometeors

During the DP event, the introduction of the on-line aerosol-IN nucleation scheme allows dust aerosols to alter the distribution of cloud hydrometeors. Figure 3 shows the DP-event-averaged vertical distributions of hydrometeors in T_{CTL} and T_{IN}, as well as their difference (T_{IN} – T_{CTL}), by using budget analysis. Figure 4 shows the differences in the production rates of different hydrometeors (T_{IN} – T_{CTL}).

Cloud ice

In layer A, when dust aerosols are considered, the IN number concentration decreases in T_{IN} (Fig. 2c), resulting in cloud ice number concentrations in T_{IN} that are approximately 5 L⁻¹ lower than those in T_{CTL}, about 40% of T_{CTL} (Fig. 3d).

Formatted: Font: 10 pt, (Asian) Chinese (Simplified, Mainland China)

480 The cloud ice mass concentration is reduced to only 10% - 50% of T_CTL (Fig. 3a,3b).
Because the two primary processes contributing to cloud ice formation in this layer—
heterogeneous nucleation and deposition-sublimation of cloud ice —are both
suppressed (Fig. 4a), and the total production rate of cloud ice (Pigen+Pidep-Psaut-
Praci-Psaci-Pgaci) drops to less than 24% of that in T_CTL. On the one hand, the
nucleated IN number concentration decreases, weakening the Pigen in T_IN by 1–2
orders of magnitude relative to T_CTL. On the other hand, the reduction in cloud ice
number concentration allows the ice crystals to grow more efficiently, with their
effective particle size generally reaching 98%-135% of that in T_CTL. The combined
485 effect of these two factors ultimately limits the deposition of water vapor onto the ice
crystals. Consequently, Pidep decreases to 20%–50% of T_CTL, with the maximum
suppression occurring at approximately 7–8 km (Fig. 4a).

490 In layer B, cloud ice number concentrations in T_IN range from 7 to 10 L⁻¹,
approximately 120% of those in T_CTL. However, the cloud ice mass concentration in
T_IN is reduced to only 70%–90% of T_CTL. The effective diameters of cloud ice also
decrease to only 77%–97% of T_CTL, with occasional reductions exceeding 50%. This
reduction is mainly attributable to combined effects of enhanced heterogeneous
nucleation and suppressed depositional growth, and the total production rate of cloud
ice drops to less than 82% of that in T_CTL. Dust aerosols provide additional ice nuclei,
495 leading to a substantial enhancement of heterogeneous nucleation in T_IN and the
formation of a much larger number of newly formed small ice crystals, with Pigen
exceeding that in T_CTL by more than two orders of magnitude. However, the increase
in cloud ice number concentration is accompanied by a reduction in individual particle
size, which limits the deposition of water vapor onto ice crystals. As a result, Pidep in
500 T_IN is reduced to about 30% of that in T_CTL, indicating that growth of cloud ice via
depositional processes is inhibited.

Snow

In layer A, the total snow production rate in T_IN increases to approximately 88%
-200% of that in T_CTL (Psdep+Paacw+Psaut+Piacr+Praci+Psaci+Psacr-Pgaut-Pracs,

505 Fig. 4b), leading to an increase in snow mass concentration to 120%–200% of T_CTL
(Fig. 3a, 3b). This increase results from the combined effects of enhanced production
rate for deposition-sublimation of snow (Psdep) and weakened production rate for
aggregation of cloud ice to snow (Psaut) and production rate for accretion of cloud ice
by snow (Psaci). The Psdep can reach approximately 2–5 times that in T_CTL (Fig. 4b).
510 In WDM6, the deposition growth of ice-phase hydrometeors is constrained by the
available water vapor, with cloud ice deposition given priority and snow deposition
consuming the remaining vapor. Because Pidep is reduced to about 20%–50% of that
in T_CTL, more water vapor is allocated to snow deposition, Psdep is then enhanced.
Meanwhile, as cloud ice reduces, Psaut and Psaci are weakened in T_IN, with both
515 processes reduced to approximately 40%–60% of their values in T_CTL (Fig. 4a, 4b).
Despite the suppression of these source terms, the substantial enhancement of snow
deposition growth dominates the snow budget in layer A, resulting in a net increase in
snow production and cloud-snow mass concentration. Finally, the ratio of cloud ice to
cloud snow changes from 1:1 to 1:3 in layer A, more closely consistent with observation,
520 which shows that cloud ice generally has higher number concentrations but lower mass
concentrations than cloud snow (Gao et al., 2020; Yang et al., 2021; Feng et al., 2021;
Fang et al., 2022).

In layer B, the snow mass concentration shows relatively small changes, ranging
from approximately 90% to 100% of T_CTL. From the perspective of cloud
525 microphysics, the mechanisms are similar to those in layer A. Despite the reduction of
Pidep, the Psdep increases to 130%–200% of T_CTL. At the same time, the decrease
in cloud ice mass leads to the continued suppression of Psaut and Psaci, resulting in a
total snow production rate of about 95% of T_CTL.

In layer C, although the model diagnostics indicate an enhancement in cloud-snow
530 production processes (production rate for accretion of rain by snow (Psacr) and
production rate for accretion of rain by cloud ice (Piacr)) and a reduction in the
production rate for accretion of snow by rain (Pracs), newly formed cloud snow cannot
be maintained because the temperature is already above 0 °C which makes it

535 instantaneously melt, rapidly converting to rain. As a result, there is no significant change in snow mass concentration in this layer.

Cloud water and rainwater

540 Cloud water and rainwater are mainly distributed in layer C (temperature approximately -2 °C to 18 °C). In this layer, both cloud-water and rainwater mixing ratios in T_IN are about 90%-95% of those in T_CTL. This small reduction is primarily attributed to a weakening of the production rate for cloud droplet activation from CCN (P_{act}), which decreases by about 5% in T_IN relative to T_CTL, indicating a suppressed conversion of water vapor into liquid water. As a consequence of the reduced cloud-water content, the production rate for accretion of rainwater by cloud water (P_{acw}) is also weakened, by 5%–10%. Meanwhile, the conversion of rainwater into ice-phase hydrometeors (P_{saci}, P_{gaci}, and P_{iaci}) is enhanced. However, under the thermodynamic conditions of layer C, temperatures exceed the melting thresholds of ice-phase hydrometeors, the newly formed snow and graupel rapidly melt and are easily converted back into rainwater. Consequently, these ice-phase conversion processes contribute only marginally to the net change in rainwater mixing ratio.

550 Overall, dust suppresses cloud development, reducing the total ice-phase hydrometeor content in layer A to 70 – 85% of T_CTL, the total ice-phase hydrometeor content in layer B to 85 – 91% of T_CTL, and the liquid-phase hydrometeor content in layer C to 90 – 95% of T_CTL. Our results indicate that dust aerosols tend to suppress cloud development in springtime dust-related precipitation over East Asia, where precipitation is predominantly stratiform. Similar suppression effects have also been reported in previous observational studies (Wang et al., 2022b; Zhu et al., 2023).~~the development of the precipitation system is suppressed (Wang et al., 2022b; Zhu et al., 2023). The on-line aerosol-IN nucleation scheme can modify the distribution of hydrometeors. Figure 3 shows the event averaged vertical distribution of hydrometeors at DPA stations simulated by T_CTL and T_CCNIN. Figure 4 shows the differences of hydrometeors between T_CTL and T_CCNIN and between T_CCN and T_CCNIN. The hydrometeor variations are further compared across three distinct phases: the 6-~~

Formatted: Not Highlight

Formatted: Not Highlight

Formatted: Font color: Auto

hour pre-precipitation (phase 1), the active precipitation period (phase 2), and the 6-hour post-precipitation (phase 3).

565 During all phase, dust aerosols suppress the formation of ice phase hydrometeors within the 0 to -40°C temperature layer. The distribution of ice phase hydrometeors in T_CCN is similar to that in T_CTL, with ice phase hydrometeor concentrations ranging around $0.27\text{--}0.50\text{ g kg}^{-1}$ within the 0 to -40°C temperature layer during phase 1–3 (Fig. 3a–f). The highest concentration of ice phase hydrometeors is in phase 1 (Fig. 3a, d). In T_CCNIN, the mixing ratio of ice phase hydrometeors decreases to 76–93% of those in T_CCN and T_CTL (Fig. 4a–f). This reduction occurs because below 6 km, the average temperature of T_CCNIN is higher than that of both the T_CCN and T_CTL by about $0.1\text{ to }0.5^{\circ}\text{C}$. This is consistent with other works which also show that as cloud top temperatures are higher in dusty conditions, more small-sized ice phase cloud particles are formed, which could limit ice phase hydrometeor development (Huang et al., 2006; Li and Min, 2010).

570 Within the 0 to -40°C temperature layer, in T_CCNIN, cloud ice mixing ratio decreases by about $0.05\text{--}0.10\text{ g kg}^{-1}$ and cloud snow increases by about $0.02\text{--}0.10\text{ g kg}^{-1}$, comparing to that of T_CTL and T_CCN during all phase (Fig. 4a–f). This is because as the cloud ice increases, the production rate for accretion of cloud ice by snow is enhanced. As a result, cloud ice is rapidly transformed into snow, leading to higher snow mass concentrations. Below the altitude of 10 km, the mean mass ratio of cloud ice to snow changes from 1:1 to 1:3, aligning more closely with observation, which shows that cloud ice generally has higher number concentrations but lower mass concentrations than cloud snow (Gao et al., 2020; Yang et al., 2021; Feng et al., 2021; Fang et al., 2022). This simulated ratio also agrees well with other numerical modeling results (Zhang et al., 2021; Park and Lim, 2023).

585 During all the three phases, dust aerosols leads to the accumulation of cloud water near the 0°C level (Fig4 a–f). In the T_CCNIN, cloud water increases by approximately $0.02\text{--}0.04\text{ g/kg}$ compared to T_CTL, and by $0.01\text{--}0.03\text{ g/kg}$ compared to T_CCN. The increasing dust IN promotes the formation of cloud ice, which subsequently transforms

Formatted: Indent: First line: 0 ch

into cloud water near the 0°C level, resulting in enhanced cloud water accumulation in DPA, which is consistent with radar-based findings reported by Zhu et al. (2023).

During phase 1, cloud water and rain water in T_CCNIN are reduced by about 0.01 g/kg⁻¹ and during phase 2 and 3, cloud water and rain water in T_CCNIN are reduced by about 0.02 g/kg⁻¹, compared to T_CTL and T_CCN (Fig. 3b,e, e, f). This is because dust INs compete with CCNs for available water vapor. As production rate for heterogeneous nucleation of cloud ice increases, the development of the precipitation system is suppressed (Wang et al., 2022b; Zhu et al., 2023).

3.3 Precipitation

The on-line aerosol-IN nucleation scheme can modulate the spatial distribution of precipitation. Figure 5a shows the observed event-accumulated precipitation of DPA stations, and Figure 5b shows the simulated event-accumulated precipitation of T_CTL. In T_CTL, 18 of 43 stations in DPA exhibit overestimated simulation precipitation compared to observations (overestimated stations), primarily located in areas near dust sources area such as Gansu, Ningxia, Shaanxi, and Inner Mongolia, as well as northeastern provinces including Shandong, Liaoning, Jilin, and Heilongjiang (Fig.5b). At these overestimated stations, the observed mean accumulated precipitation is 11.499.98 mm, while the simulated mean accumulated precipitation is 25.55 mm (Fig.6), with an average sMAPE of 4542.98%. The other 25 stations show underestimated simulated precipitation compared to observations (underestimated stations), mainly distributed across Hebei, Beijing, Henan, and the Yangtze River Basin downwind area of the dust events (Fig.5b). At underestimated stations, the observed mean accumulated precipitation is 31.5831.86 mm (Fig.6), while the simulated value is only 4.63 mm, with an average sMAPE of -64%.5.52 mm, with an average sMAPE of -64.39%.

In T_CCN, on-line aerosol-CCN cloud interaction scheme can improve the underestimation of precipitation simulation in areas such as Beijing, Shanxi, Hebei, and Hubei (Fig. 5c). For underestimated stations, mean accumulated precipitation increases by 0.52 mm compared to that of T_CTL (Fig. 6). However, underestimation of

Formatted: Font: (Asian) 宋体, 小四

625 precipitation becomes more severe in Anhui, Jiangsu, Shandong, Sichuan, Chongqing,
and parts of Hubei, resulting in no significant improvement in MAE, RMSE and
sMAPE (Fig. 7b). For underestimated stations, precipitation simulation improves by
approximately 1.57% in T_CCN. For overestimated stations, the simulation
630 performance deteriorated compared to T_CTL; the mean accumulated precipitation is
1.11 mm higher than that in T_CTL (Fig. 6), and precipitation simulation deteriorates
by approximately 11%, with MAE increasing by 1.1 and RMSE by 2.1 (Fig. 7a).
Overall, precipitation simulation is improved in 22 of 43 stations. It shows that only the
influence of CCN by aerosols can introduce some more bias to make those stations
performance worse.

In T_CCNIN, the on-line aerosol-IN nucleation scheme does not alter the overall
pattern of overestimation precipitation north of 35° N and underestimation precipitation
to the south of 35° N in T_CTL (Fig. 5d). However, compared to T_CTL, notable
improvements are mainly observed primarily between 34° and 40° N. This is driven
635 by the process discussed in Section 3.2, where the presence of dust in layer C suppresses
P_{act}, thereby reducing the overestimation of precipitation near the dust source
areas. As discussed in Section 3.2, dust IN competes with CCN for water vapor at layer
with temperature above 0°C, suppressing precipitation and reducing the overestimation
of precipitation near the dust source areas. sMAPE is reduced by about 1–10 % in areas
640 near the dust source area, resulting in more accurate forecasts compared to both T_CTL
and T_CCN (Fig. 5e, f).

645 Rather than being removed by precipitation or evaporation, the suppressed cloud
hydrometeors are transported downstream in T_IN. We calculate horizontal
hydrometeor fluxes across 116°E, 33°–50°N and 33°N, 103°–116°E from 12:00 UTC
on 12 April to 18:00 UTC on 13 April (Fig. 6). Over the entire 0–12 km layer, the total
hydrometeor flux slightly increases to about 102% of that in T_CTL.

Within the temperature range from 0 to -40 °C, the total horizontal hydrometeor
flux decreases by about 11 %, primarily due to a substantial reduction in cloud ice flux,
accompanied by increases in snow and graupel fluxes. In Layer A, the total hydrometeor

Formatted: Font: (Default) Times New Roman, (Asian) 宋体, 小四, Font color: Auto, Pattern: Clear

Formatted: Font: (Default) Times New Roman, (Asian) 宋体, 小四, Font color: Auto, Pattern: Clear

Formatted: Font: (Default) Times New Roman, (Asian) 宋体, 小四, Font color: Auto, Pattern: Clear

Formatted: Font: (Default) Times New Roman, (Asian) 宋体, 小四, Font color: Auto, Pattern: Clear

Formatted: Font: (Default) Times New Roman, (Asian) 宋体

650 flux is about $4.4 \times 10^{-5} \text{ kg s}^{-1}$, corresponding to about 75 % of T_CTL. Cloud ice flux
drops sharply to about 8 % of T_CTL, while snow and graupel fluxes increase markedly
to about 19.8 times and 7.8 times, respectively. In Layer B, the total hydrometeor flux
is about $2.6 \times 10^{-6} \text{ kg s}^{-1}$, corresponding to about 93 % of T_CTL, with cloud ice flux
655 reduced to about 28 % of T_CTL, and snow and graupel fluxes increased to about 2.3
times and about 1.8 times, respectively. At temperatures above 0 °C, the total horizontal
hydrometeor flux increases to about 106 % of T_CTL, with cloud water and rainwater
fluxes increasing to about 115 % and about 108 %, respectively.

These results indicate that although dust suppresses cold-cloud development in the
upper and mid-troposphere, it enhances the downstream transport of liquid-phase
660 hydrometeors near and below the melting layer, enhancing downstream
precipitation. Rather than being removed by precipitation or evaporation, the suppressed
cloud water is transported downstream in T_CCNIN,

665 Finally, for improving underestimation precipitation simulations over areas such as
Beijing and Shanxi, where sMAPE is reduced by 5–77 % (Fig. 5e). Compared with
T_CCN, T_CCNIN not only improves precipitation simulations between 34° and 40° N,
but also shows improvements over Sichuan and Hubei. However, it suppresses
precipitation over the Yangtze River Basin, resulting in increased model simulation
error there (Fig. 5f). For underestimation stations, the mean accumulated precipitation
increases by ~~0.18~~1.1 mm compared to T_CCNCTL, and precipitation simulations
670 improves by approximately ~~0.64~~%, with little changes in MAE and RMSE (Fig. 67b).
For overestimated stations, the mean accumulated precipitation decreases by ~~4.54~~5 mm
compared to T_CTLCCN, and precipitation simulations improves by approximately
40%, with MAE reduced by 1.4 and RMSE reduced by 4.1 (Fig. 7a) approximately 15%,
with MAE reduced by 0.8 and RMSE reduced by 3.2 (Fig. 6a).

675 In summary, because the reduction in cloud water in the 0–4 km layer is relatively
small, the corresponding decrease in rainwater reaching the surface is also limited. As
a result, the on-line aerosol-IN nucleation scheme exerts only a weak influence on the
total precipitation amount. Nevertheless, it can modulate the spatial and temporal

Formatted

Formatted: Indent: First line: 0 ch

Formatted: Not Highlight

distribution of precipitation, impressing overestimated and altering underestimation in a degree, which is consistent with the findings of Park and Lim (2023) and Su and Fung (2018b). In all, precipitation simulations at 24 of 43 stations in T_CCNIN show improvement compared to both T_CTL and T_CCN.

Formatted: Not Highlight

Formatted: Not Highlight

Formatted: Not Highlight

In summary, while the on-line aerosol-IN nucleation scheme has limited impact on the total precipitation amount, it modulates the spatial and temporal distribution of precipitation, same to that of Park and Lim (2023) and Su and Fung (2018b). Dust aerosols suppress precipitation near source areas; the suppressed cloud water can be conserved within the weather system and transported to downwind areas where it can enhance the precipitation efficiency there. This redistribution of precipitation improves the performance of the GRAPES/CUACE.

Formatted: Indent: First line: 0 ch

4 Conclusions and discussion

Formatted: Font: 10 pt, (Asian) Chinese (Simplified, Mainland China)

In order to explore the impact of spring dust aerosols on precipitation, in GRAPES/CUACE, this study has improved the WDM6 scheme to predict both cloud ice number and mass concentrations. And we also develop an on-line aerosol-IN nucleation scheme in the regional model GRAPES/CUACE. The model performance has been evaluated by a typical dust-precipitation event from 00:00 UTC on 9 April to 00:00 UTC on 15 April 2018.

Dust provides ice nuclei by heterogeneous nucleation during dust-precipitation event. The on-line aerosol-IN nucleation scheme significantly modifies nucleated IN concentration distributions. The original WDM6 scheme exhibits a systematic underestimation of ice nuclei concentrations, with nucleated IN concentrations can reach $10^2 L^{-1}$ between 4 and 7 km altitude during the dust-precipitation event, and abnormally increase with height due to the temperature-dependent formulation of original WDM6 scheme, peaking near the $-40^\circ C$ layer. With the on-line aerosol-IN nucleation scheme, IN concentrations can reach $10^4 L^{-1}$, so for the cloud ice mass production rate concentrated peaking at about the layer between 4 and 7 km in height, more closer to the observations

Formatted: Superscript

Formatted: Superscript

Dust can inhibit the development of clouds. Above 7 km, dust suppresses the

Formatted: Indent: First line: 2 ch

710 growth rate of cloud ice (through both heterogeneous nucleation and deposition-
sublimation rate of cloud ice), and the total production rate of cloud ice drops to less
than 24% of that in T_CTL, promoting snow formation and ultimately reducing the
total ice-phase hydrometeor content to 70–85% of T_CTL. Meanwhile, the total snow
production rate in T_IN increases to approximately 88% - 200% of that in T_CTL,
reducing total ice-phase hydrometeor content to 70 - 85% of T_CTL. Between 4 and
7 km height, dust enhances heterogeneous nucleation of cloud ice, but the new smaller
715 particles suppress cloud ice and reduces the deposition rate, resulting in the total ice-
phase hydrometeor content decreasing to 85–91% of T_CTL. Below 4 km in height,
dust slightly suppresses the conversion of water vapor to cloud water and of cloud water
to rain, reducing the liquid-phase hydrometeor content to 90–95% of T_CTL.

720 The dust can also modulate the spatial distribution of precipitation even though
the on-line aerosol-IN nucleation scheme cannot alter completely the overall pattern of
overestimation precipitation north of 35° N and underestimation precipitation to the
south of 35° N as seen in T_CTL. The on-line aerosol-IN nucleation scheme
significantly modifies IN concentration distributions. The original WDM6 scheme
exhibits a systematic underestimation of ice nuclei concentrations, with IN
725 concentrations ranging around $10^0 - 10^1 L^{-1}$ between 3 and 5 km altitude during the
dust precipitation event, and abnormally increasing vertically due to the temperature-
dependent nature of original WDM6 scheme, peaking near the $-40^\circ C$ layer. With the
on-line aerosol-IN nucleation scheme, IN concentrations reached $10^2 - 10^4 L^{-1}$
between 3 and 5 km altitude, peaking at about the layer between 4 and 5 km in height,
730 and cloud ice is concentrated between 2 and 6 km, which agrees better with observation.

735 The on-line aerosol-IN nucleation scheme alters the cloud hydrometeor
distributions. Within the $-40^\circ C$ to $0^\circ C$ temperature layer, dust suppresses the formation
of ice-phase hydrometeors. The mixing ratio of ice-phase hydrometeors decreases to
76–93% of those in T_CCN and T_CTL. This reduction occurs because during dusty
conditions cloud-top temperatures are higher and more small-sized ice-phase cloud
particles formed, both of which could limit ice-phase hydrometeor development. The

on-line aerosol-IN nucleation scheme ultimately leads the average ratio of cloud ice to cloud snow changing from 1:1 to 1:3, which is much closer to the observation. This is because that the production rate for accretion of cloud ice by snow also rises as the production rate for nucleation of ice increases, enhancing the accretion of cloud ice to snow.

In the temperature layer above 0°C, increased cloud ice converts to cloud water near the 0°C temperature layer, resulting in the accumulation of cloud water at layers near the 0°C temperature layer. Compared to T_CCN, cloud water increases by about 0.02-0.04 g/kg by competing for available water vapor between CCN and IN. The increasing production rate for nucleation of ice suppress the precipitation, leading cloud water and rain water are reduced by approximately 0.02 g kg⁻¹ during the active precipitation period.

The on-line aerosol-IN nucleation scheme can also modulate the spatial distribution of precipitation. In this case, the on-line aerosol-IN nucleation scheme and the on-line aerosol-CCN cloud interaction scheme does not alter the overall pattern of overestimation precipitation north of 35°N and underestimation precipitation to the south of 35°N as seen in T_CTL. Only considering the influence of CCN by aerosols further increases the bias at DPA stations where precipitation simulation was originally inaccurate.

After comprehensively considering aerosol effects on both IN and CCN, The on-line aerosol-IN nucleation scheme mitigates the overestimation of precipitation near dust source areas. ~~he on-line aerosol-IN nucleation scheme mitigates the overestimation of rainfall in these areas by suppressing precipitation near dust source areas.~~ For overestimated stations, the event-mean accumulated precipitation decreases by about 41.5 mm relative to compared to T_CCNCTL, with the MAE reduces by 0.81.4 and the RMSE reduces by 3.24.1. ~~Meanwhile, However,~~ the cloud hydrometeors ~~water~~ suppressed by dust IN ~~is are~~ not removed from the atmosphere; instead, ~~it they~~ remains in the weather system and transported releases ~~releases~~ downstream as the air mass moves, thereby alleviating improving ~~improving~~ the underestimation of precipitation in

Formatted: Font: (Default) Times New Roman, (Asian) 宋体, 小四

Formatted: Font: (Default) Times New Roman, (Asian) 宋体, 小四

Formatted: Font: (Default) Times New Roman, (Asian) 宋体, 小四

Formatted: Font: (Default) Times New Roman, (Asian) 宋体, 小四

Formatted: Font: (Default) Times New Roman, (Asian) 宋体, 小四

downstream areas. In stations where precipitation is previously underestimated, the mean accumulated precipitation increases by about ~~0.18~~1.1 mm relative to T_CTLF_CCN.

This study shows ~~comprehensive improvements~~positive impacts of dust as IN aerosol on cloud and precipitation simulation by a comprehensive online aerosol-~~CCN~~-IN-cloud interaction scheme. Considering both CCN and IN effects, rather than CCN alone, improves precipitation simulations by up to approximately 40 %.~~It also shows that considering aerosols' impact only on warm cloud water process can actually increase model inaccuracies, and comprehensively accounting for aerosol effects on both CCN and IN improves precipitation simulations by approximately up to 15 %.~~ Aerosol and clouds interactions are an old open question, but there are still many uncertainties, due to the complex mechanisms of both CCN and IN. Furthermore, the scarcity of real-time observations hinders the in-depth exploration of detailed microphysical processes and their underlying mechanisms. More cases in different seasons and different dusty cases are needed to perform in the future with more observations.~~As the interactions are influenced by both the aerosols and precipitation weather conditions, more cases in different season and different dusty cases are needed to perform in the near future.~~

Formatted: Font color: Auto

Formatted: Font: (Default) Times New Roman, (Asian) 宋体, 小四, Font color: Auto, Pattern: Clear

Code/data availability

All source code and data can be accessed by contacting the corresponding author Chunhong Zhou (zhouch@cma.gov.cn).

Author contributions.

JZ developed the on-line aerosol-IN nucleation scheme, conducted the data analysis, and wrote the original draft of this paper. CHZ developed the aerosol-CCN-cloud interaction scheme and the on-line aerosol-IN nucleation scheme, and reviewed and edited the manuscript, providing critical insights. XYS reviewed the manuscript. HW reviewed the manuscript and provided general insight. SLG reviewed the manuscript. XYZ reviewed the manuscript and gave guidance on the data analysis. All authors have given approval to the final version of the paper.

795 **Competing interests**

The authors declare that they have no conflict of interest.

Financial support.

This study was jointly supported by the NSFC Project (42090030) and the National Key Project of the Ministry of Science and Technology of China (2022YFC3701205).

800 **Acknowledgment.**

All figures in this study were produced by the open-source software of MeteoInfoLab from <http://www.meteothink.org/index.html>. The meteorological initial and boundary conditions for the modeling system were obtained from the China Meteorological Data Sharing Service System (<http://data.cma.cn/data/cdcindex/cid/98c64da7ee348b37> html). The meteorological observations were obtained from the China Meteorological Data Sharing Service System (<http://data.cma.cn/data/cdcindex/cid/f0fb4b55508804ca> html). The PM₁₀ and PM_{2.5} concentration data from the national environmental monitoring network of the Ministry of Ecology and Environment of China (<http://www.cnemc.cn>), [The NCEP/NCAR Final Operational Global Analysis \(FNL\) data, with a temporal resolution of 6 hours and a spatial resolution of 0.25 °](#) (<https://rda.ucar.edu/datasets/ds083.3/>).

Formatted: Font: (Default) Times New Roman, (Asian) 宋体, 小四

Formatted: Font: (Asian) 宋体, 小四

Formatted: Not Superscript/ Subscript

Formatted: Font: (Default) Times New Roman, (Asian) 宋体, 小四

Formatted: Font: 小四, Not Highlight

Formatted: Font: 小四, Not Highlight

References

Albrecht, B. A.: Aerosols, Cloud Microphysics, and Fractional Cloudiness, *Science*, 245, 1227–1230, <https://doi.org/10.1126/science.245.4923.1227>, 1989.

815 Alfaro, S. and Gomes, L.: Modeling mineral aerosol production by wind erosion: Emission intensities and aerosol size distributions in source areas, *Journal of Geophysical Research*, 106, 18075–18084, <https://doi.org/10.1029/2000JD900339>, 2001.

Andreae, M. O. and Crutzen, P. J.: Atmospheric Aerosols: Biogeochemical Sources and Role in Atmospheric Chemistry, *Science*, 276, 1052–1058, <https://doi.org/10.1126/science.276.5315.1052>, 1997.

820 Boose, Y., Welti, A., Atkinson, J., Ramelli, F., Danielczok, A., Bingemer, H. G., Plötze, M., Sierau, B., Kanji, Z. A., and Lohmann, U.: Heterogeneous ice nucleation on dust particles sourced from nine deserts worldwide – Part 1: Immersion freezing, *Atmospheric Chemistry and Physics*, 16, 15075–15095, <https://doi.org/10.5194/acp-16-15075-2016>, 2016.

825 Cantrell, W., Bunker, K., Niehaus, J., China, S., Woodward, X., Kostinski, A., and Mazzoleni, C.: Ice nucleation in the contact mode: Temperature and size dependence for selected dusts, *AIP Conference Proceedings*, 1527, 926–931, <https://doi.org/10.1063/1.4803423>, 2013.

Cao, G., Zhang, X., and Zheng, F.: Inventory of black carbon and organic carbon emissions from

Formatted: Font: (Default) Times New Roman

- China, *Atmospheric Environment*, 40, 6516–6527,
830 <https://doi.org/10.1016/j.atmosenv.2006.05.070>, 2006.
- Cao, G.-L., Zhang, X., Wang, D., and Zheng, F.-C.: Inventory of atmospheric pollutants discharged from biomass burning in China continent, *China Environ*, 25, 389–393, 2005.
- Che, Y., Zhang, J., Zhao, C., Fang, W., Xue, W., Yang, W., Ji, D., Dang, J., Duan, J., Sun, J., Shen, X., and Zhou, X.: A study on the characteristics of ice nucleating particles concentration and aerosols and their relationship in spring in Beijing, *Atmospheric Research*, 247, 105196,
835 <https://doi.org/10.1016/j.atmosres.2020.105196>, 2021.
- Chen, D., Xue, J., Yang, X., Zhang, H., Shen, X., Hu, J., Wang, Y., Ji, L., and Chen, J.: New generation of multi-scale NWP system (GRAPES): General scientific design, *Chinese Science Bulletin*, 53, 3433–3445, <https://doi.org/10.1007/s11434-008-0494-z>, 2008.
- 840 Chen, J., Wu, Z., Chen, J., Reicher, N., Fang, X., Rudich, Y., and Hu, M.: Size-resolved atmospheric ice-nucleating particles during East Asian dust events, *Atmospheric Chemistry and Physics*, 21, 3491–3506, <https://doi.org/10.5194/acp-21-3491-2021>, 2021.
- Chen, J., Wu, Z., Meng, X., Zhang, C., Chen, J., Qiu, Y., Chen, L., Fang, X., Wang, Y., Zhang, Y., Chen, S., Gao, J., Li, W., and Hu, M.: Observational evidence for the non-suppression effect of atmospheric chemical modification on the ice nucleation activity of East Asian dust, *Sci Total Environ*, 861, 160708, <https://doi.org/10.1016/j.scitotenv.2022.160708>, 2023.
- DeMott, P. J., Prenni, A. J., Liu, X., Kreidenweis, S. M., Petters, M. D., Twohy, C. H., Richardson, M. S., Eidhammer, T., and Rogers, D. C.: Predicting global atmospheric ice nuclei distributions and their impacts on climate, *Proceedings of the National Academy of Sciences*, 107, 11217–
850 11222, <https://doi.org/10.1073/pnas.0910818107>, 2010.
- DeMott, P. J., Prenni, A. J., McMeeking, G. R., Sullivan, R. C., Petters, M. D., Tobo, Y., Niemand, M., Möhler, O., Snider, J. R., Wang, Z., and Kreidenweis, S. M.: Integrating laboratory and field data to quantify the immersion freezing ice nucleation activity of mineral dust particles, *Atmospheric Chemistry and Physics*, 15, 393–409, <https://doi.org/10.5194/acp-15-393-2015>,
855 2015.
- Eastwood, M. L., Cremel, S., Gehrke, C., Girard, E., and Bertram, A. K.: Ice nucleation on mineral dust particles: Onset conditions, nucleation rates and contact angles, *Journal of Geophysical Research: Atmospheres*, 113, <https://doi.org/10.1029/2008JD010639>, 2008.
- 860 Fan, J., Leung, L. R., DeMott, P. J., Comstock, J. M., Singh, B., Rosenfeld, D., Tomlinson, J. M., White, A., Prather, K. A., Minnis, P., Ayers, J. K., and Min, Q.: Aerosol impacts on California winter clouds and precipitation during CalWater 2011: local pollution versus long-range transported dust, *Atmospheric Chemistry and Physics*, 14, 81–101, <https://doi.org/10.5194/acp-14-81-2014>, 2014.
- Fang, W., Lou, X., Zhang, X., and Fu, Y.: Numerical Simulations of Cloud Number Concentration and Ice Nuclei Influence on Cloud Processes and Seeding Effects, *Atmosphere*, 13, 1792, <https://doi.org/10.3390/atmos13111792>, 2022.
- 865 Feng, Q., Niu, S., Niu, T., Fan, X., Shen, D., and Yang, J.: Aircraft—Based Observation of the Physical Characteristics of Snowfall Cloud in Shanxi Province, *Chinese Journal of Atmospheric Sciences (in Chinese)*, 45, 1146–1160, <https://doi.org/10.3878/j.issn.1006-9895.2106.21004> 2021.
- 870 Filonchyk, M., Yan, H., Shareef, T. M. E., and Yang, S.: Aerosol contamination survey during dust storm process in Northwestern China using ground, satellite observations and atmospheric

- modeling data, *Theor Appl Climatol*, 135, 119–133, <https://doi.org/10.1007/s00704-017-2362-8>, 2019.
- 875 Gao, Q., Guo, X., He, H., Liu, X., Huang, M., and Ma, X.: Numerical Simulation Study on the Microphysical Characteristics of Stratiform Clouds with Embedded Convections in Northern China based on Aircraft Measurements, *Chinese Journal of Atmospheric Sciences*(in Chinese), 44, 899–912, <https://doi.org/10.3878/j.issn.1006-9895.1908.19114>, 2020.
- 880 Gibbons, M., Min, Q., and Fan, J.: Investigating the impacts of Saharan dust on tropical deep convection using spectral bin microphysics, *Atmospheric Chemistry and Physics*, 18, 12161–12184, <https://doi.org/10.5194/acp-18-12161-2018>, 2018.
- Gong, S. L. and Zhang, X. Y.: CUACE/Dust - an integrated system of observation and modeling systems for operational dust forecasting in Asia, *Atmospheric Chemistry and Physics*, 8, 2333–2340, <https://doi.org/10.5194/acp-8-2333-2008>, 2008.
- 885 Gong, S. L., Zhang, X. Y., Zhao, T. L., McKendry, I. G., Jaffe, D. A., and Lu, N. M.: Characterization of soil dust aerosol in China and its transport and distribution during 2001 ACE-Asia: 2. Model simulation and validation, *Journal of Geophysical Research: Atmospheres*, 108, <https://doi.org/10.1029/2002JD002633>, 2003.
- 890 Haerig, M., Ansmann, A., Walser, A., Baars, H., Urbanneck, C., Weinzierl, B., Schöberl, M., Dollner, M., Mamouri, R., and Althausen, D.: Estimation of dust related ice nucleating particles in the atmosphere: Comparison of profiling and in-situ measurements, *E3S Web Conf.*, 99, 04002, <https://doi.org/10.1051/e3sconf/20199904002>, 2019.
- Han, Y., CHEN, Y., Fang, X., and Zhao, T.: The possible effect of dust aerosol on precipitation in Tarim basin., *China Environmental Science*, 28(2), 102–106, <https://doi.org/10.3321/j.issn:1000-6923.2008.02.002>, 2008.
- 895 He, Y., Zhang, Y., Liu, F., Yin, Z., Yi, Y., Zhan, Y., and Yi, F.: Retrievals of dust-related particle mass and ice-nucleating particle concentration profiles with ground-based polarization lidar and sun photometer over a megacity in central China, *Atmospheric Measurement Techniques*, 14, 5939–5954, <https://doi.org/10.5194/amt-14-5939-2021>, 2021.
- 900 He, C., Yin, Y., Huang, Y., Kuang, X., Cui, Y., Chen, K., Jiang, H., Kiselev, A., Möhler, O., and Schrod, J.: The Vertical Distribution of Ice-Nucleating Particles over the North China Plain: A Case of Cold Front Passage, *Remote Sensing*, 15, 4989, <https://doi.org/10.3390/rs15204989>, 2023.
- 905 Herbert, R. J., Sanchez-Marroquin, A., Grosvenor, D. P., Pringle, K. J., Arnold, S. R., Murray, B. J., and Carslaw, K. S.: Gaps in our understanding of ice-nucleating particle sources exposed by global simulation of the UK Earth System Model, *Atmospheric Chemistry and Physics*, 25, 291–325, <https://doi.org/10.5194/acp-25-291-2025>, 2025.
- 910 Hiranuma, N., Augustin-Bauditz, S., Bingemer, H., Budke, C., Curtius, J., Danielczok, A., Diehl, K., Dreischmeier, K., Ebert, M., Frank, F., Hoffmann, N., Kandler, K., Kiselev, A., Koop, T., Leisner, T., Möhler, O., Nillius, B., Peckhaus, A., Rose, D., Weinbruch, S., Wex, H., Boose, Y., DeMott, P. J., Hader, J. D., Hill, T. C. J., Kanji, Z. A., Kulkarni, G., Levin, E. J. T., McCluskey, C. S., Murakami, M., Murray, B. J., Niedermeier, D., Petters, M. D., O’Sullivan, D., Saito, A., Schill, G. P., Tajiri, T., Tolbert, M. A., Welti, A., Whale, T. F., Wright, T. P., and Yamashita, K.: A comprehensive laboratory study on the immersion freezing behavior of illite NX particles: a comparison of 17 ice nucleation measurement techniques, *Atmospheric Chemistry and Physics*, 15, 2489–2518, <https://doi.org/10.5194/acp-15-2489-2015>, 2015.
- 915

Formatted: Font: (Default) Times New Roman

- Hong, S.-Y., Dudhia, J., and Chen, S.-H.: A Revised Approach to Ice Microphysical Processes for the Bulk Parameterization of Clouds and Precipitation, *Monthly Weather Review*, 132, 103–120, [https://doi.org/10.1175/1520-0493\(2004\)132<0103:ARATIM>2.0.CO;2](https://doi.org/10.1175/1520-0493(2004)132<0103:ARATIM>2.0.CO;2), 2004.
- 920 Hong, S.-Y., Noh, Y., and Dudhia, J.: A New Vertical Diffusion Package with an Explicit Treatment of Entrainment Processes, *Monthly Weather Review*, 134, 2318–2341, <https://doi.org/10.1175/MWR3199.1>, 2006.
- Hu, Y., Tian, P., Huang, M., Bi, K., Schneider, J., Umo, N. S., Ullmerich, N., Höhler, K., Jing, X., Xue, H., Ding, D., Liu, Y., Leisner, T., and Möhler, O.: Characteristics of ice-nucleating particles in Beijing during spring: A comparison study of measurements between the suburban and a nearby mountain area, *Atmospheric Environment*, 293, 119451, <https://doi.org/10.1016/j.atmosenv.2022.119451>, 2023.
- 925 Huang, J., Minnis, P., Lin, B., Wang, T., Yi, Y., Hu, Y., Sun-Mack, S., and Ayers, K.: Possible influences of Asian dust aerosols on cloud properties and radiative forcing observed from MODIS and CERES, *Geophysical Research Letters*, 33, <https://doi.org/10.1029/2005GL024724>, 2006.
- 930 Iltoviz, E., Khain, A. P., Benmoshe, N., Phillips, V. T. J., and Ryzhkov, A. V.: Effect of Aerosols on Freezing Drops, Hail, and Precipitation in a Midlatitude Storm, *Journal of the Atmospheric Sciences*, 73, 109–144, <https://doi.org/10.1175/JAS-D-14-0155.1>, 2016.
- 935 Jiang, H., Yin, Y., Wang, X., Gao, R., Yuan, L., Chen, K., and Shan, Y.: The measurement and parameterization of ice nucleating particles in different backgrounds of China, *Atmospheric Research*, 181, 72–80, <https://doi.org/10.1016/j.atmosres.2016.06.013>, 2016.
- Kang, J.-Y., Yoon, S., Shao, Y., and Kim, S.-W.: Comparison of vertical dust flux by implementing three dust emission schemes in WRF/Chem, *Journal of Geophysical Research*, 116, <https://doi.org/10.1029/2010JD014649>, 2011.
- 940 Kang, Y., Jin, S., Peng, X., Yang, X., Shang, K., and Wang, S.: Comparative Analysis of Single-Moment and Double-Moment Microphysics Schemes in WRF on the Torrential Rainfall Event in North China During 1921 July, 2016, *Plateau Meteorology*, 37, 481–494, <https://doi.org/10.7522/j.issn.1000-0534.2017.00026>, 2018.
- 945 Kanji, Z. A., Ladino, L. A., Wex, H., Boose, Y., Burkert-Kohn, M., Cziczo, D. J., and Krämer, M.: Overview of Ice Nucleating Particles, *Meteorological Monographs*, 58, <https://doi.org/10.1175/AMSMONOGRAPHS-D-16-0006.1>, 2017.
- Kaufman, Y. J., Tanré, D., and Boucher, O.: A satellite view of aerosols in the climate system, *Nature*, 419, 215–223, <https://doi.org/10.1038/nature01091>, 2002.
- 950 Khain, A., Ovtchinnikov, M., Pinsky, M., Pokrovsky, A., and Krugliak, H.: Notes on the state-of-the-art numerical modeling of cloud microphysics, *Atmospheric Research*, 55, 159–224, [https://doi.org/10.1016/S0169-8095\(00\)00064-8](https://doi.org/10.1016/S0169-8095(00)00064-8), 2000.
- Khain, A. P., Beheng, K. D., Heymsfield, A., Korolev, A., Krichak, S. O., Levin, Z., Pinsky, M., Phillips, V., Prabhakaran, T., Teller, A., van den Heever, S. C., and Yano, J.-I.: Representation of microphysical processes in cloud-resolving models: Spectral (bin) microphysics versus bulk parameterization, *Reviews of Geophysics*, 53, 247–322, <https://doi.org/10.1002/2014RG000468>, 2015.
- 955 Knopf, D. A. and Alpert, P. A.: Atmospheric ice nucleation, *Nat Rev Phys*, 5, 203–217, <https://doi.org/10.1038/s42254-023-00570-7>, 2023.
- 960 Kwon, J., Lim, K.-S. S., Park, S.-Y., Kim, K., and Lee, G.: Effects of Prognostic Number

Formatted: Font: (Default) Times New Roman

Formatted: Font: (Default) Times New Roman

- Concentrations of Snow and Graupel on the Simulated Precipitation over the Korean Peninsula, *Nature Mater*, 15, 1113–1119, <https://doi.org/10.1175/WAF-D-23-0057.1>, 2023.
- 965 Lee, S. S., Kim, B.-G., Yum, S. S., Seo, K.-H., Jung, C.-H., Um, J. S., Li, Z., Hong, J., Chang, K.-H., and Jeong, J.-Y.: Effects of aerosol on evaporation, freezing and precipitation in a multiple cloud system, *Clim Dyn*, 48, 1069–1087, <https://doi.org/10.1007/s00382-016-3128-1>, 2017.
- Li, J., Liu, W., Castarède, D., Gu, W., Li, L., Ohigashi, T., Zhang, G., Tang, M., Thomson, E. S., Hallquist, M., Wang, S., and Kong, X.: Hygroscopicity and Ice Nucleation Properties of Dust/Salt Mixtures Originating from the Source of East Asian Dust Storms, *Front. Environ. Sci.*, 10, <https://doi.org/10.3389/fenvs.2022.897127>, 2022.
- 970 Li, M., Zhang, Q., Kurokawa, J., Woo, J.-H., He, K., Lu, Z., Ohara, T., Song, Y., Streets, D. G., Carmichael, G. R., Cheng, Y., Hong, C., Huo, H., Jiang, X., Kang, S., Liu, F., Su, H., and Zheng, B.: MIX: a mosaic Asian anthropogenic emission inventory under the international collaboration framework of the MICS-Asia and HTAP, *Atmospheric Chemistry and Physics*, 17, 935–963, <https://doi.org/10.5194/acp-17-935-2017>, 2017.
- 975 Li, R. and Min, Q.-L.: Impacts of mineral dust on the vertical structure of precipitation, *Journal of Geophysical Research: Atmospheres*, 115, <https://doi.org/10.1029/2009JD011925>, 2010.
- Marticorena, B. and Bergametti, G.: Modeling the atmospheric dust cycle: 1. Design of a soil-derived dust emission scheme, *Journal of Geophysical Research: Atmospheres*, 100, 16415–16430, <https://doi.org/10.1029/95JD00690>, 1995.
- 980 Mascioli, N. R., Evan, A. T., and Ralph, F. M.: Influence of Dust on Precipitation During Landfalling Atmospheric Rivers in an Idealized Framework, *Journal of Geophysical Research: Atmospheres*, 126, e2021JD034813, <https://doi.org/10.1029/2021JD034813>, 2021.
- Molthan, A. L. and Colle, B. A.: Comparisons of Single- and Double-Moment Microphysics Schemes in the Simulation of a Synoptic-Scale Snowfall Event, *Monthly Weather Review*, 140, 2982–3002, <https://doi.org/10.1175/MWR-D-11-00292.1>, 2012.
- 985 Naeger, A. R.: Impact of dust aerosols on precipitation associated with atmospheric rivers using WRF-Chem simulations, *Results in Physics*, 10, 217–221, <https://doi.org/10.1016/j.rinp.2018.05.027>, 2018.
- Nenes, A., Murray, B., and Bougiatioti, A.: Mineral Dust and its Microphysical Interactions with Clouds, *Mineral Dust: A Key Player in the Earth System*, 287–325, https://doi.org/10.1007/978-94-017-8978-3_12, 2014.
- 990 Niehaus, J., Becker, J. G., Kostinski, A., and Cantrell, W.: Laboratory Measurements of Contact Freezing by Dust and Bacteria at Temperatures of Mixed-Phase Clouds, *Journal of the Atmospheric Sciences*, 71, 3659–3667, <https://doi.org/10.1175/JAS-D-14-0022.1>, 2014.
- 995 Pan, X., Uno, I., Wang, Z., Nishizawa, T., Sugimoto, N., Yamamoto, S., Kobayashi, H., Sun, Y., Fu, P., Tang, X., and Wang, Z.: Real-time observational evidence of changing Asian dust morphology with the mixing of heavy anthropogenic pollution, *Sci Rep*, 7, 335, <https://doi.org/10.1038/s41598-017-00444-w>, 2017.
- 1000 Park, S.-Y. and Lim, K.-S. S.: Implementation of Prognostic Cloud Ice Number Concentrations for the Weather Research and Forecasting (WRF) Double-Moment 6-Class (WDM6) Microphysics Scheme, *Journal of Advances in Modeling Earth Systems*, 15, e2022MS003009, <https://doi.org/10.1029/2022MS003009>, 2023.
- Patnaude, R. J., McCluskey, C. S., Roberts, G. C., DeMott, P. J., Hill, T. C. J., McFarquhar, G. M., Kollias, P., Ranjbar, K., Wolde, M., and Kreidenweis, S. M.: Characteristics of Ice Nucleating

Formatted: Font: (Default) Times New Roman

- 1005 Particles From the Long-Range Transport of Saharan Dust, *Geophysical Research Letters*, 52, e2024GL113365, <https://doi.org/10.1029/2024GL113365>, 2025.
- Possner, A., Ekman, A. M. L., and Lohmann, U.: Cloud response and feedback processes in stratiform mixed-phase clouds perturbed by ship exhaust, *Geophysical Research Letters*, 44, 1964–1972, <https://doi.org/10.1002/2016GL071358>, 2017.
- 1010 Ramanathan, V., Crutzen, P., Kiehl, J., and Rosenfeld, D.: Aerosols, Climate, and the Hydrological Cycle, *Science*, 294, 2119–24, <https://doi.org/10.1126/science.1064034>, 2001.
- Rosenfeld, D. and Bell, T. L.: Why do tornados and hailstorms rest on weekends?, *Journal of Geophysical Research: Atmospheres*, 116, <https://doi.org/10.1029/2011JD016214>, 2011.
- Shao, Y., Ishizuka, M., Mikami, M., and Leys, J. F.: Parameterization of size-resolved dust emission and validation with measurements, *Journal of Geophysical Research: Atmospheres*, 116, <https://doi.org/10.1029/2010JD014527>, 2011.
- 1015 Shcherbakov, M., Brebels, A., Shcherbakova, N. L., Tyukov, A., Janovsky, T. A., and Kamaev, V. A.: A survey of forecast error measures, *World Applied Sciences Journal*, 24, 171–176, <https://doi.org/10.5829/idosi.wasj.2013.24.itmies.80032>, 2013.
- 1020 Shen X., Shi Y., Wang H., Zhang M., and Han J.: Comparison of two double-moment cloud microphysics schemes in the GRAPES_Meso model on simulating a cold cloud process, *Torrential Rain and Disasters*, 41, 336–347, <https://doi.org/10.3969/j.issn.1004-9045.2022.03.010>, 2022.
- Shen, X., Mei, H., Wang, W., and Huang, W.: Numerical Simulation of Ice-Phase Processes Using a Double-Moment Microphysical Scheme and a Sensitivity Test of Ice Nuclei Concentration, *Chinese Journal of Atmospheric Sciences*, 39, 83–99, <https://doi.org/10.3878/j.issn.1006-9895.1405.13310>, 2015.
- 1025 Stevens, R. G., Loewe, K., Dearden, C., Dimitrelos, A., Possner, A., Eirund, G. K., Raatikainen, T., Hill, A. A., Shipway, B. J., Wilkinson, J., Romakkaniemi, S., Tonttila, J., Laaksonen, A., Korhonen, H., Connolly, P., Lohmann, U., Hoose, C., Ekman, A. M. L., Carslaw, K. S., and Field, P. R.: A model intercomparison of CCN-limited tenuous clouds in the high Arctic, *Atmospheric Chemistry and Physics*, 18, 11041–11071, <https://doi.org/10.5194/acp-18-11041-2018>, 2018.
- 1030 Stier, P., van den Heever, S. C., Christensen, M. W., Gryspeerdt, E., Dagan, G., Saleeby, S. M., Bollasina, M., Donner, L., Emanuel, K., Ekman, A. M. L., Feingold, G., Field, P., Forster, P., Haywood, J., Kahn, R., Koren, I., Kummerow, C., L'Ecuyer, T., Lohmann, U., Ming, Y., Myhre, G., Quaas, J., Rosenfeld, D., Samset, B., Seifert, A., Stephens, G., and Tao, W.-K.: Multifaceted aerosol effects on precipitation, *Nat. Geosci.*, 17, 719–732, <https://doi.org/10.1038/s41561-024-01482-6>, 2024.
- 1035 Stith, J. L., Ramanathan, V., Cooper, W. A., Roberts, G. C., DeMott, P. J., Carmichael, G., Hatch, C. D., Adhikary, B., Twohy, C. H., Rogers, D. C., Baumgardner, D., Prenni, A. J., Campos, T., Gao, R., Anderson, J., and Feng, Y.: An overview of aircraft observations from the Pacific Dust Experiment campaign, *Journal of Geophysical Research: Atmospheres*, 114, <https://doi.org/10.1029/2008JD010924>, 2009.
- 1040 Su, L. and Fung, J. C. H.: Investigating the role of dust in ice nucleation within clouds and further effects on the regional weather system over East Asia – Part 1: model development and validation, *Atmospheric Chemistry and Physics*, 18, 8707–8725, <https://doi.org/10.5194/acp-18-8707-2018>, 2018a.
- 1045

- 1050 Su, L. and Fung, J. C. H.: Investigating the role of dust in ice nucleation within clouds and further effects on the regional weather system over East Asia – Part 2: modification of the weather system, *Atmospheric Chemistry and Physics*, 18, 11529–11545, <https://doi.org/10.5194/acp-18-11529-2018>, 2018b.
- 1055 Tobo, Y., Adachi, K., DeMott, P. J., Hill, T. C. J., Hamilton, D. S., Mahowald, N. M., Nagatsuka, N., Ohata, S., Uetake, J., Kondo, Y., and Koike, M.: Glacially sourced dust as a potentially significant source of ice nucleating particles, *Nat. Geosci.*, 12, 253–258, <https://doi.org/10.1038/s41561-019-0314-x>, 2019.
- Tobo, Y., Uetake, J., Matsui, H., Moteki, N., Uji, Y., Iwamoto, Y., Miura, K., and Misumi, R.: Seasonal Trends of Atmospheric Ice Nucleating Particles Over Tokyo, *Journal of Geophysical Research: Atmospheres*, 125, <https://doi.org/10.1029/2020JD033658>, 2020.
- 1060 Trochkin, D., Iwasaka, Y., Matsuki, A., Yamada, M., Kim, Y.-S., Nagatani, T., Zhang, D., Shi, G.-Y., and Shen, Z.: Mineral aerosol particles collected in Dunhuang, China, and their comparison with chemically modified particles collected over Japan, *Journal of Geophysical Research: Atmospheres*, 108, <https://doi.org/10.1029/2002JD003268>, 2003.
- 1065 Twomey, S.: The Influence of Pollution on the Shortwave Albedo of Clouds., *Journal of the Atmospheric Sciences*, 34, 1149–1154, [https://doi.org/10.1175/1520-0469\(1977\)034<1149:TIOPOT>2.0.CO;2](https://doi.org/10.1175/1520-0469(1977)034<1149:TIOPOT>2.0.CO;2), 1977.
- Um, J., McFarquhar, G. M., Stith, J. L., Jung, C. H., Lee, S. S., Lee, J. Y., Shin, Y., Lee, Y. G., Yang, Y. I., Yum, S. S., Kim, B.-G., Cha, J. W., and Ko, A.-R.: Microphysical characteristics of frozen droplet aggregates from deep convective clouds, *Atmospheric Chemistry and Physics*, 18, 16915–16930, <https://doi.org/10.5194/acp-18-16915-2018>, 2018.
- 1070 Wang, H., Gong, S. L., Zhang, H. L., Chen, Y., Shen, X. S., Chen, D. H., Xue, J. S., Shen, Y. F., and Jin, W. Z.: A new-generation sand and dust storm forecasting system GRAPES_CUACE/Dust: Model development, verification and numerical simulation, *Chinese Science Bulletin*, 55, 635–649, <https://doi.org/10.1007/s11434-009-0481-z>, 2010.
- 1075 Wang, H., Zhang, X. Y., Wang, P., Peng, Y., Zhang, W. J., Liu, Z. D., Han, C., Li, S. T., Wang, Y. Q., Che, H. Z., Huang, L. P., Liu, H. L., Zhang, L., Zhou, C. H., Ma, Z. S., Chen, F. F., Ma, X., Wu, X. J., Zhang, B. H., and Shen, X. S.: Chemistry-Weather Interacted Model System GRAPES_Meso5.1/CUACE CW V1.0: Development, Evaluation and Application in Better Haze/Fog Prediction in China, *Journal of Advances in Modeling Earth Systems*, 14, e2022MS003222, <https://doi.org/10.1029/2022MS003222>, 2022a.
- 1080 Wang, W.: Observation and study on the transport of dust aerosol and its climate effect., Doctoral dissertation, Lanzhou University, 2013.
- 1085 Wang, W., Sheng, L., Jin, H., and Han, Y.: Dust aerosol effects on cirrus and altocumulus clouds in Northwest China, *J Meteorol Res*, 29, 793–805, <https://doi.org/10.1007/s13351-015-4116-9>, 2015.
- Wang, Y. and Yan, Z.: Effect of Different Verification Schemes on Precipitation Verification and Assessment Conclusion, *Meteorological Monthly*, 33, 53-61, <https://doi.org/10.3969/j.issn.1000-0526.2007.12.008>, 2007.
- 1090 Wang, Z., Xue, L., Liu, J., Ding, K., Lou, S., Ding, A., Wang, J., and Huang, X.: Roles of Atmospheric Aerosols in Extreme Meteorological Events: a Systematic Review, *Curr Pollution Rep*, 8, 177–188, <https://doi.org/10.1007/s40726-022-00216-9>, 2022b.
- Xu, G. Q., Chen, D. H., Xue, J. S., Sun, J., and Wang, S. Y.: The program structure designing and

- optimizing tests of GRAPES physics, *Chinese Science Bulletin*, 53, 3470–3476, <https://doi.org/10.1007/s11434-008-0418-y>, 2008.
- 1095 Yang, J., Hu, X., Lei, H., Duan, Y., Lv, F., and Zhao, L.: Airborne Observations of Microphysical Characteristics of Stratiform Cloud Over Eastern Side of Taihang Mountains, *Chinese Journal of Atmospheric Sciences*, 45(1), 88–106, <https://doi.org/10.3878/j.issn.1006-9895.2004.19202>, 2021.
- 1100 Zhang, M., Yu, H., Guo, J., Shen, X., Su, Y., Xue, H., and Dou, B.: Assessment on Unsystematic Errors of GRAPES_GFS 2.0, *Journal of Applied Meteorological Science*, 30, 332–344, <https://doi.org/10.11898/1001-7313.20190307>, 2019.
- 1105 Zhang, W., Wang, H., Zhang, X., Huang, L., Peng, Y., Liu, Z., Zhang, X., and Che, H.: Aerosol–cloud interaction in the atmospheric chemistry model GRAPES_Meso5.1/CUACE and its impacts on mesoscale numerical weather prediction under haze pollution conditions in Jing–Jin–Ji in China, *Atmospheric Chemistry and Physics*, 22, 15207–15221, <https://doi.org/10.5194/acp-22-15207-2022>, 2022.
- 1110 Zhang, Y., Yu, F., Luo, G., Fan, J., and Liu, S.: Impacts of long-range-transported mineral dust on summertime convective cloud and precipitation: a case study over the Taiwan region, *Atmospheric Chemistry and Physics*, 21, 17433–17451, <https://doi.org/10.5194/acp-21-17433-2021>, 2021.
- Zhang, Z. and Shen, X.: On the development of the GRAPES—A new generation of the national operational NWP system in China, *Chinese Science Bulletin*, 53, 3429–3432, <https://doi.org/10.1007/s11434-008-0462-7>, 2008.
- 1115 Zhou, C., Zhang, X., Gong, S., Wang, Y., and Xue, M.: Improving aerosol interaction with clouds and precipitation in a regional chemical weather modeling system, *Atmospheric Chemistry and Physics*, 16, 145–160, <https://doi.org/10.5194/acp-16-145-2016>, 2016.
- Zhou, C., Gui, H., Hu, J., Ke, H., Wang, Y., and Zhang, X.: Detection of New Dust Sources in Central/East Asia and Their Impact on Simulations of a Severe Sand and Dust Storm, *Journal of Geophysical Research: Atmospheres*, 124, 10232–10247, <https://doi.org/10.1029/2019JD030753>, 2019.
- 1120 Zhou, C. H., Gong, S., Zhang, X.Y., Liu, H. L., Xue, M., Cao, G. L., An, X. Q., Che, H. Z., Zhang, Y. M., and Niu, T.: Towards the improvements of simulating the chemical and optical properties of Chinese aerosols using an online coupled model – CUACE/Aero, *Tellus B: Chemical and Physical Meteorology*, 64, 18965, <https://doi.org/10.3402/tellusb.v64i0.18965>, 2012.
- 1125 Zhou, Z., Yin, C., Lu, C., Jia, X., Ye, F., Qiu, Y., and Cheng, M.: Large Eddy Simulation of Microphysics and Influencing Factors in Shallow Convective Clouds, *Atmosphere*, 12, 485, <https://doi.org/10.3390/atmos12040485>, 2021.
- 1130 Zhou C., Rao X., Sheng L., Zhang J., Lu, Lin J., Hu J., Zhang B., and Xu R.: Application of Scale-adaptive Dust Emission Scheme to CMA-CUACE/Dust, *J Appl Meteor Sci*, 35, 400–413, <https://doi.org/10.11898/1001-7313.20240402>, 2024.
- Zhu, H., Li, R., Yang, S., Zhao, C., Jiang, Z., and Huang, C.: The impacts of dust aerosol and convective available potential energy on precipitation vertical structure in southeastern China as seen from multisource observations, *Atmospheric Chemistry and Physics*, 23, 2421–2437, <https://doi.org/10.5194/acp-23-2421-2023>, 2023.
- 1135

Formatted: Font: (Default) Times New Roman

Formatted: Font: (Default) Times New Roman

Figure

Figure 1

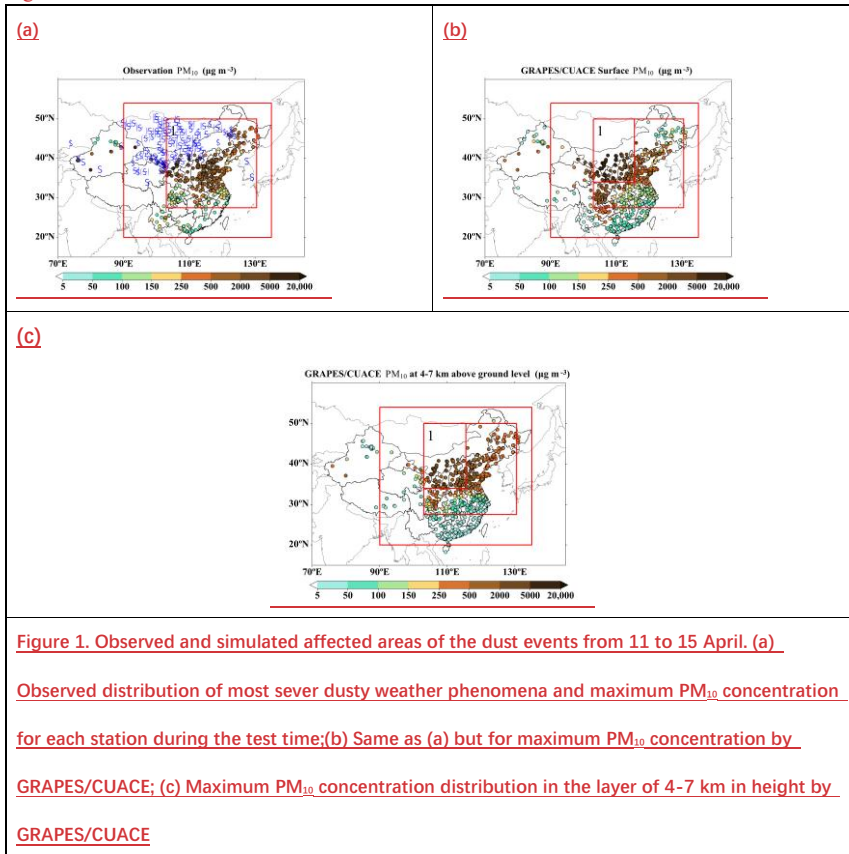


Figure 1. Observed and simulated affected areas of the dust events from 11 to 15 April. (a) Observed distribution of most severe dusty weather phenomena and maximum PM₁₀ concentration for each station during the test time;(b) Same as (a) but for maximum PM₁₀ concentration by GRAPES/CUACE; (c) Maximum PM₁₀ concentration distribution in the layer of 4-7 km in height by GRAPES/CUACE

Figure 2

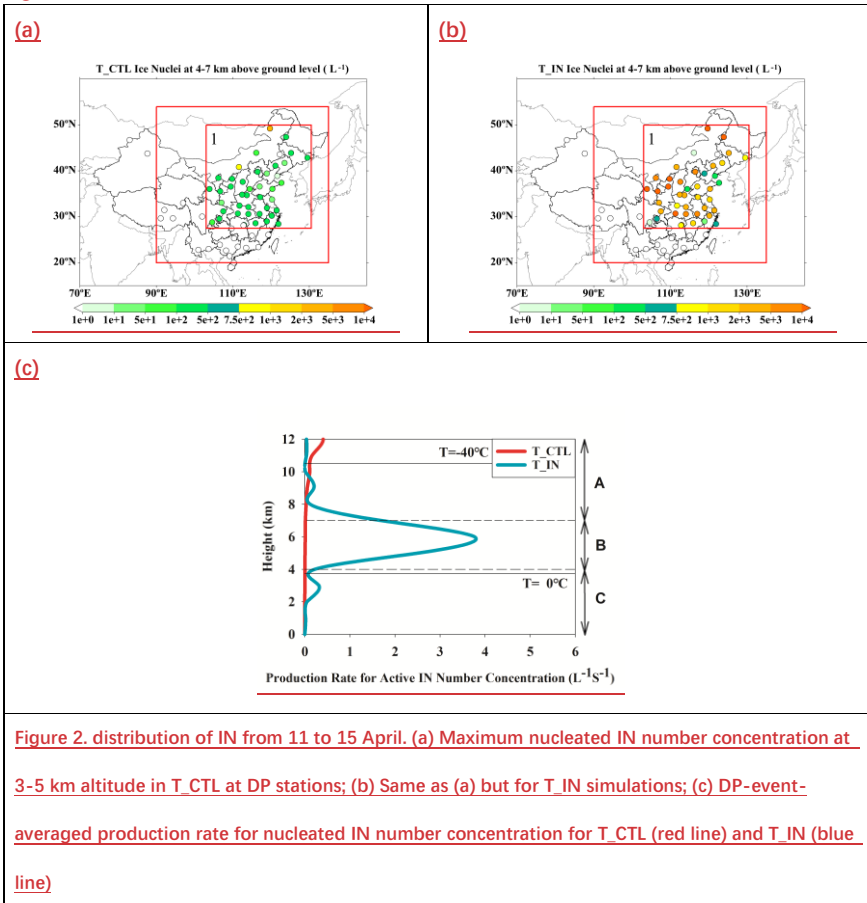


Figure 2. distribution of IN from 11 to 15 April. (a) Maximum nucleated IN number concentration at 3-5 km altitude in T_CTL at DP stations; (b) Same as (a) but for T_IN simulations; (c) DP-event-averaged production rate for nucleated IN number concentration for T_CTL (red line) and T_IN (blue line)

Figure 3

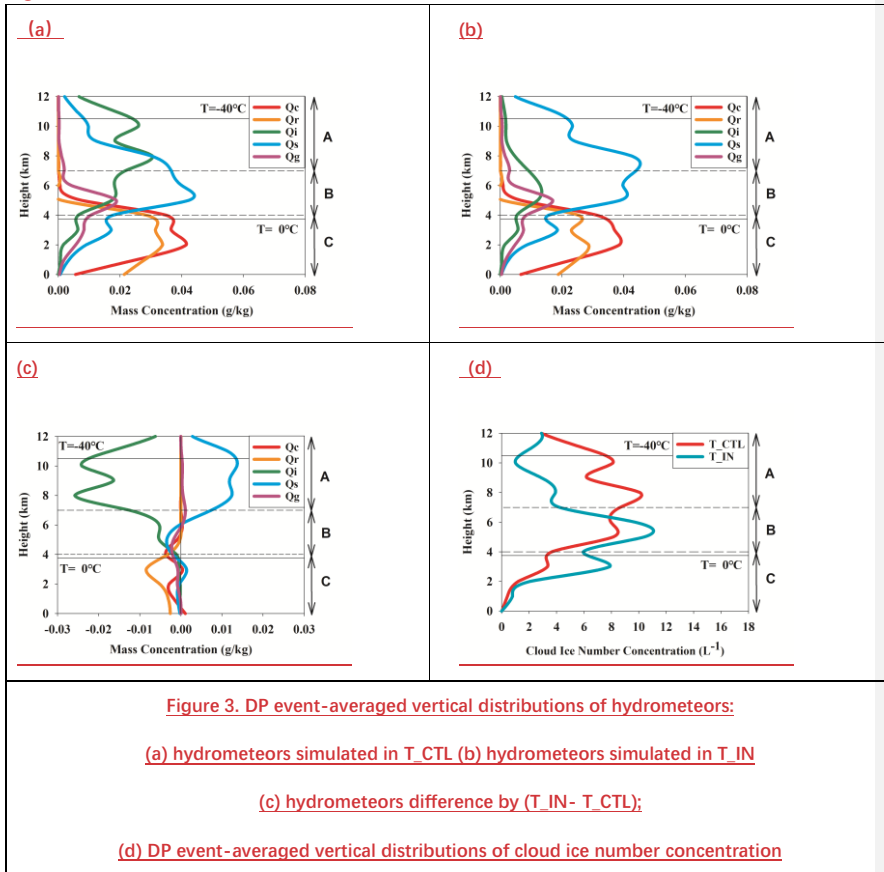


Figure 4

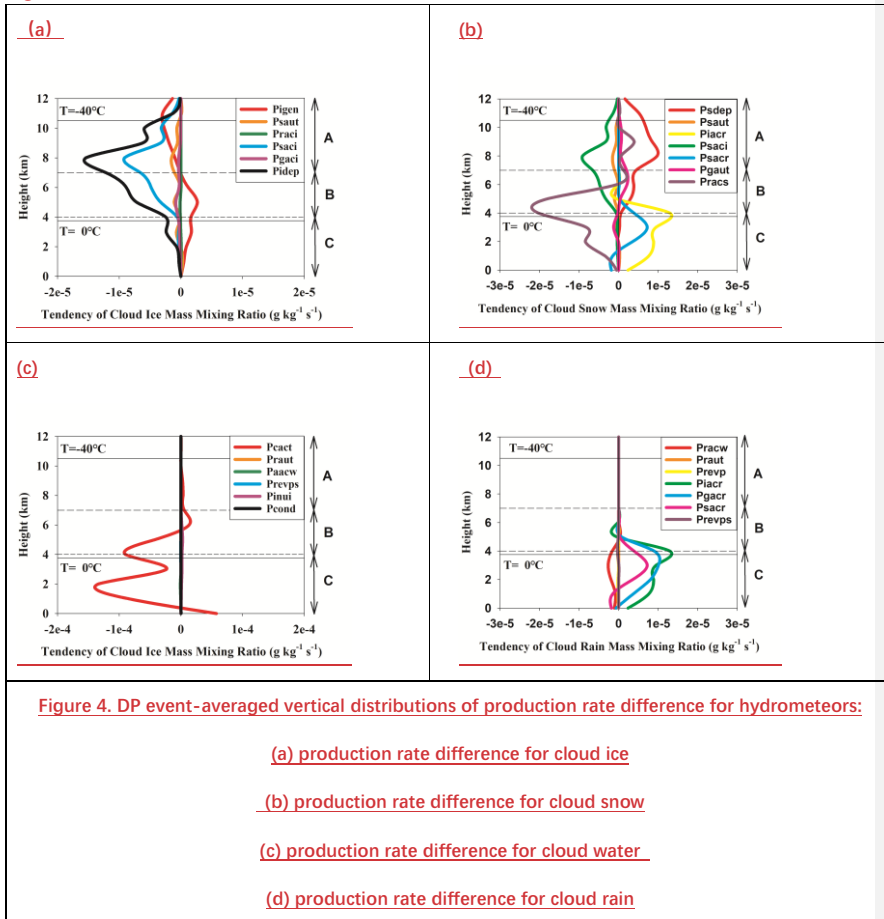


Figure 5

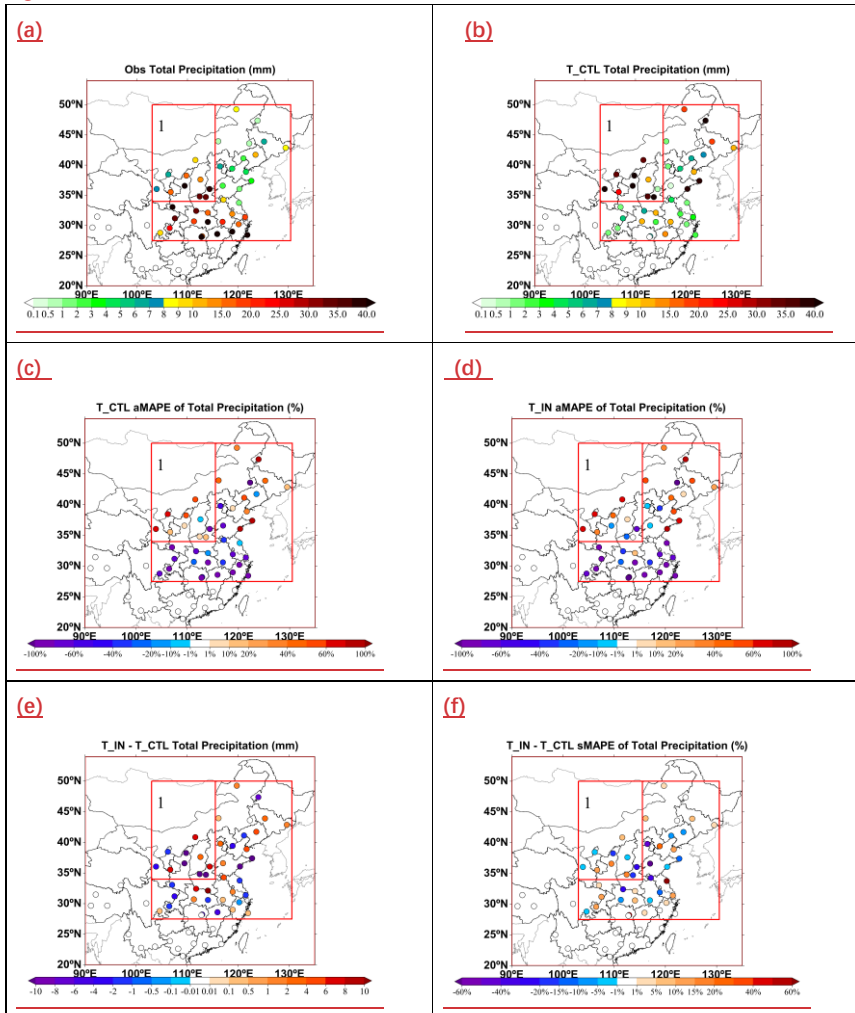


Figure 5. Comparison of observed and simulated accumulated precipitation at dust-precipitation

stations:

(a) Observed accumulated precipitation from 11th 00:00 UTC to 15th 00:00 UTC;

(b) Same as a but for T_CTL;

(c) aMAPE of simulated accumulated precipitation in T_CTL;

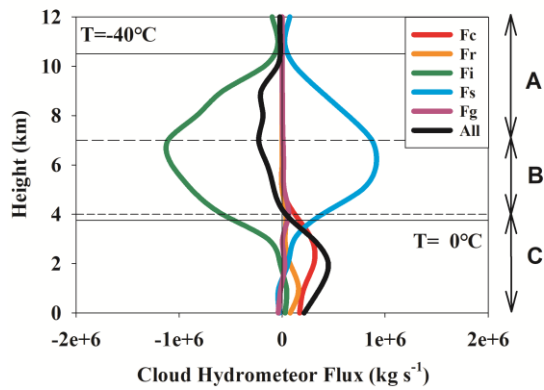
(d) aMAPE of simulated accumulated precipitation in T_IN;

(e) Difference in precipitation between T_IN and T_CTL;

(f) Difference in sMAPE between T_IN and T_CTL.

Figure 6

(a)



(b)

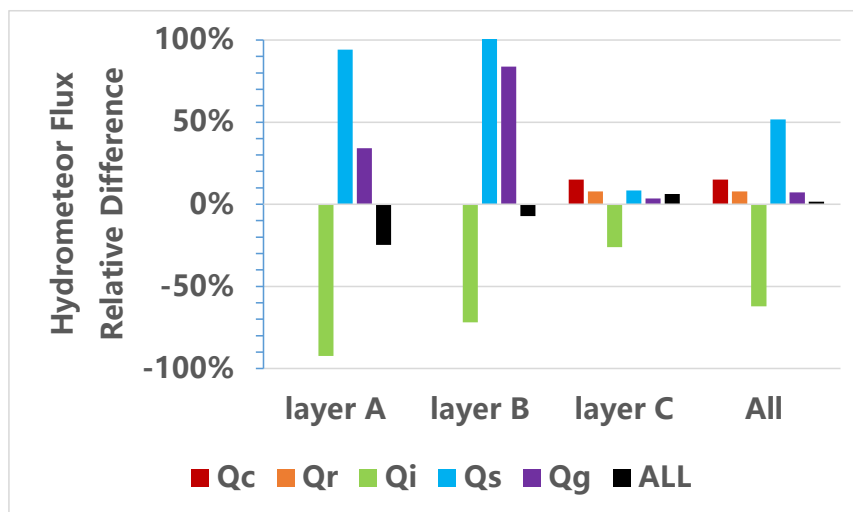


Figure 6. Horizontal hydrometeor fluxes across 116°E (33°–50°N) and 33°N (103°–116°E).

Here, Fc denotes cloud water flux, Fr rainwater flux, Fi cloud ice flux, Fs snow flux, Fg graupel flux, and All the total hydrometeor flux.

(a) Differences in horizontal hydrometeor fluxes $(T_{IN} - T_{CTL})$.

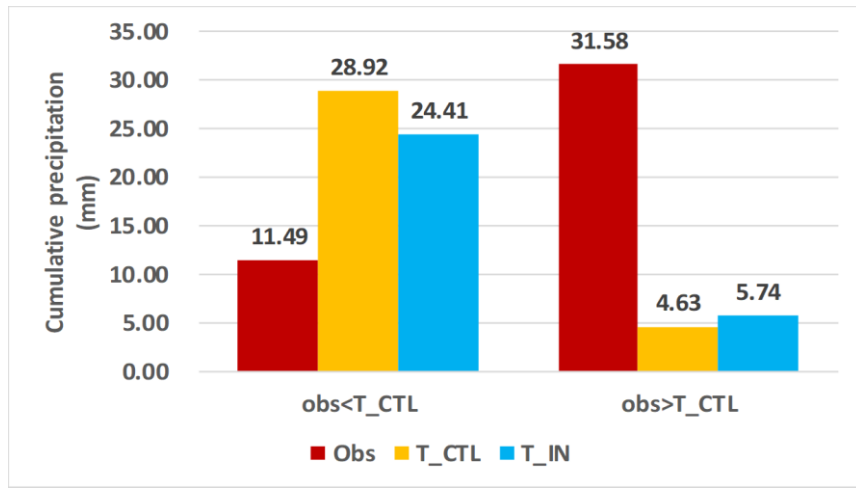
(b) Fractional changes in horizontal hydrometeor fluxes in Layers A, B, C, and the total column, defined as $(T_{IN} - T_{CTL}) / T_{CTL}$. Snow and graupel fluxes in Layer A show extremely large

1150

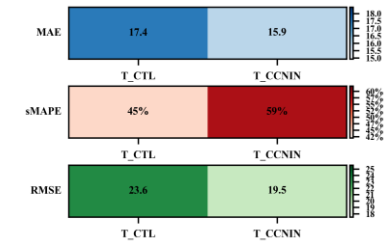
increases (about 1883 % and 683 %, respectively); for better visualization, these values are scaled down by a factor of 20 in the figure.

Figure 7

(a)



(b)



(c)

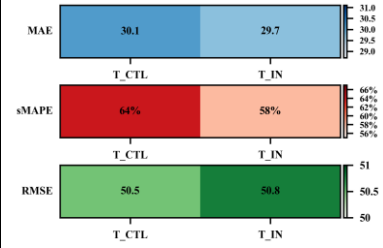


Figure 7.

(a) mean accumulated precipitation during DP event at overestimated stations and underestimated stations

(b) Statistical analysis of observed versus simulated accumulated precipitation at DPA stations for Overestimated stations

(c) same as (b), but for Underestimated stations

Table

Table 1. Three Tests designed for different types of precipitation

<u>Test</u>	<u>Warm cloud</u>	<u>Cold cloud</u>
<u>T_CTL</u>	<u>on-line aerosol-CCN interaction scheme</u>	<u>original WDM6</u>
<u>T_IN</u>	<u>on-line aerosol-CCN interaction scheme</u>	<u>on-line aerosol-IN nucleation scheme</u>

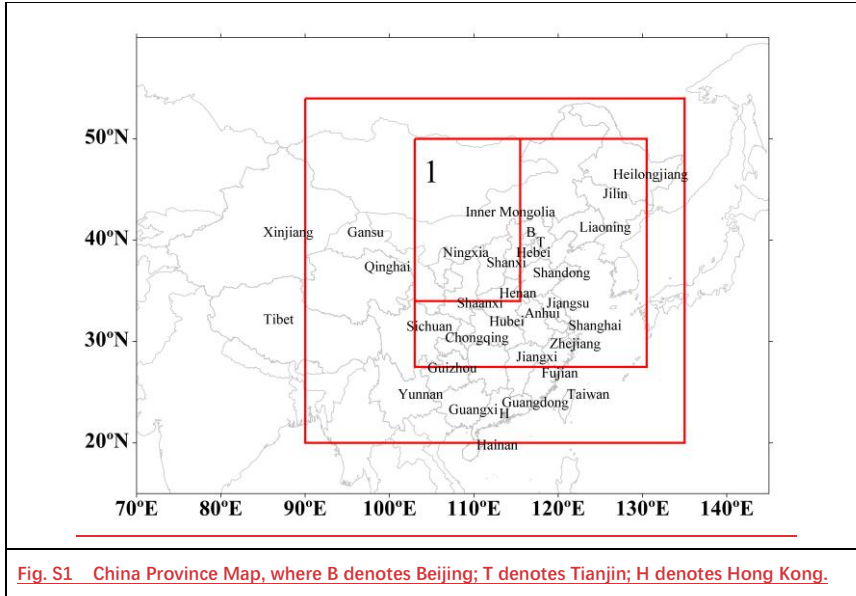
1155

Table 2. List of Symbols

<u>Symbol</u>	<u>Meaning</u>
<u>Paacw</u>	<u>Production rate for accretion of cloud water by averaged snow/graupel</u>
<u>Pcact</u>	<u>Production rate for cloud droplet activation from CCN</u>
<u>Pcond</u>	<u>Production rate for condensation rate of water vapor to cloud liquid water</u>
<u>Pgacr</u>	<u>Production rate for accretion of rain by graupel</u>
<u>Pgaci</u>	<u>Production rate for accretion of cloud ice by graupel</u>
<u>Pgaut</u>	<u>Production rate for aggregation form snow to graupel</u>
<u>Piacr</u>	<u>Production rate for accretions of rain by cloud ice</u>
<u>Pidep</u>	<u>Production rate for deposition- sublimation rate of cloud ice</u>
<u>Pigen</u>	<u>Production rate for heterogeneous nucleation</u>
<u>Pinud</u>	<u>Production rate for deposition/condensation freezing to form cloud ice</u>
<u>Pinui</u>	<u>Production rate for immersion freezing of cloud water to form cloud ice</u>
<u>Pracs</u>	<u>Production rate for accretions of cloud snow by rain</u>
<u>Pracw</u>	<u>Production rate for accretion of cloud water by rain</u>
<u>Praci</u>	<u>Production rate for accretion of cloud ice by rain</u>
<u>Praut</u>	<u>Production rate for aggregation form cloud water ice to form rain</u>
<u>Prevps</u>	<u>Production rate for evaporation/condensation rate of cloud water</u>
<u>Prevp</u>	<u>Production rate for evaporation/condensation rate of rain</u>
<u>Psacr</u>	<u>Production rate for accretions of rain by cloud snow</u>

<u>Psaci</u>	<u>Production rate for accretion of cloud ice by snow</u>
<u>Psaut</u>	<u>Production rate for aggregation form cloud ice to snow</u>
<u>Pscar</u>	<u>Production rate for accretion of rain by snow</u>
<u>Psdep</u>	<u>Production rate for deposition- sublimation rate of cloud snow</u>

Supplementary Figure 1



Formatted: Indent: Left: 0 cm, First line: 0 ch